Magmatic architecture around the Ōkataina Volcanic Centre, Taupō Volcanic Zone, Aotearoa New Zealand, inferred from basalt geochemistry

Ery C. Hughes: Te Pū Ao | GNS Science (e.hughes@gns.cri.nz)

Sally Law: School of GeoSciences, University of Edinburgh (Sally.Law@ed.ac.uk)

Geoff Kilgour: Te Pū Ao | GNS Science (g.kilgour@gns.cri.z)

Jon D. Blundy: University of Oxford (jonathan.blundy@earth.ox.ac.uk)

Heidy M. Mader: University of Bristol (h.m.mader@bristol.ac.uk)

This paper is a revised version of a non-peer review pre-print submitted to EarthArXiv, which has been submitted to the Journal of Volcanology and Geothermal Research special issue on the Okataina Volcanic Centre for peer review.

Twitter handles: @eryhughes, @sallylaw, @NZvolcanologist

Abstract

The Ōkataina Volcanic Centre (ŌVC) is the most recently active volcanic centre in the Taupō Volcanic Zone, Aotearoa New Zealand. Although best known for its high rates of explosive rhyolitic volcanism, there are several examples of basaltic to basaltic-andesite contributions to ŌVC eruptions. These range from minor involvement of basalt in rhyolitic eruptions to the exclusively basaltic 1886 C.E. Plinian eruption of Tarawera. To explore the basaltic component supplying this dominantly rhyolitic area, we analyse the textures and compositions (minerals and melt inclusions) of four basaltic eruptions from within and around the ŌVC that have similar whole rock chemistry, namely: Terrace Rd, Rotomakariri, Rotokawau, and Tarawera. Data from these basaltic deposits provide constraints on the conditions of magma evolution and ascent in the crust prior to eruption, revealing that eruptions sample multiple distinct reservoirs during ascent to the surface. The most abundant basaltic component is generated by cooling-induced crystallisation of a common, oxidised, basaltic melt at various depths within the crust. The volatile content of this melt was increased by protracted fluid-undersaturated crystallisation. Despite similar bulk compositions, comparable to other basaltic deposits in the region, these four eruptions are texturally distinct due to their wide variation in eruption style.

Keywords: geochemistry, Tarawera, Terrace Rd, Rotomakariri, Rotokawau, melt inclusion

1 Introduction

Volcanic arcs are characterised by complicated sub-surface architectures that convert basaltic mantle-derived melt into a wide variety of more evolved arc magma compositions (e.g., reviews by Ducea et al., 2015; Grove et al., 2012). Compositional variability can be derived from variations in the primary composition of the mantle melt input, extents of crustal assimilation, type of petrological processes occurring (e.g., crystallisation, degassing, mixing), and the conditions of magma stagnation (pressure, temperature). Static models drive compositional variation by changes in temperature (e.g., Annen et al., 2006), whereas dynamic models drive compositional variation by reactive melt percolation (e.g., Jackson et al., 2018); both mechanisms have been used to explain the compositional variability of arc magmas. Reconciling these models requires observations and analysis of volcanic rocks or exhumed crustal sections, which provide snapshots and time-integrated histories, respectively, of magmatic systems.

Both crustal and erupted materials at arcs are dominated by evolved magma composition (i.e., andesites to rhyolites) despite the large inputs of basaltic melt required for their formation. Most basalts never reach the surface due to relatively high magma density compared to the surrounding crust. Furthermore, these intrusions cool in the crust and either solidify to gabbroic plutons or generate more evolved magmas that separate and ascend to then erupt or cool to form felsic plutons. Periodic magma mixing (e.g., basalt with rhyolite) may be important in generating intermediate magmas and triggering eruptions (e.g., Laumonier et al., 2014; Sparks et al., 1977). Any basaltic magmas that do reach the surface will have traversed this complicated crustal region, yet unravelling this cryptic differentiation history is not trivial and inevitably requires high resolution, *in situ* mineral analysis. Here, we utilise microanalytical geochemical methods to collect data on crystals and their melt inclusions to explore the paths taken by basaltic magmas beneath a dominantly rhyolitic caldera. We aim to constrain how and where basaltic magmas are stored within the crust, and what petrological processes affect them. This is important for assessing the current state of magma reservoirs in the crust in the context of geophysical surveys and predicting potential precursory signals before a future eruption at caldera systems.

The Ōkataina Volcanic Centre (ŌVC) is one of two currently active caldera systems in the Taupō Volcanic Zone, Aotearoa New Zealand (Taupō Volcanic Centre is the other). From several studies of the rhyolites, the sub-surface architecture below the ŌVC is known to comprise discrete rhyolitic melt-mush pockets that erupt compositionally distinct magmas within single eruptions (e.g., Cole et al., 2014; Sas et al., 2021; Shane et al., 2008a, 2007; Smith et al., 2004; Storm et al., 2011). Basaltic magmas are key to generating the more evolved magma compositions in the ŌVC, but little is known about their evolution. Heat and volatiles are assumed to be transferred between basalts and rhyolites to trigger rhyolitic eruptions (e.g., Leonard et al. 2002; Shane et al. 2007, 2008; Smith et al. 2010), but the initial volatile contents of the basaltic magmas are largely unconstrained. The abundant evidence for basaltic-rhyolitic magma interaction also enables the investigation of how magma mixing is related to basaltic eruption style (e.g., Leonard et al., 2002; Shane et al., 2005). In this study, we combine textural observations with mineral and melt inclusion chemistries to constrain the magmatic compositions (including volatiles), conditions, and processes occurring during crustal storage and ascent of basaltic magmas around the ŌVC.

2 Regional setting

The Taupō Volcanic Zone (TVZ) is the most frequently active and productive silicic system on Earth (Wilson et al., 2009). Oblique subduction of the Pacific plate under continental Zealandia leads to the clockwise rotation of the eastern portion of the North Island, resulting in extension in the TVZ, crustal thinning, and basalt underplating (Houghton et al., 1995; Mortimer et al., 2017; Wilson et al., 1995). High rates of basaltic underplating drive the generation of voluminous silicic magma and, together with the relatively thin and faulted crust, enhance magma production and the high frequency of eruptions (e.g., Cole et al., 2014; Price et al., 2005). Extensive crustal contamination occurs, which influences the isotopic composition of both erupted basalts and rhyolites (e.g., Gamble et al., 1993; Graham et al., 1995; Sas et al., 2021; Waight et al., 2017).

Basalt scoria cones and tuffs are volumetrically minor surface features, being one and two-to-three orders of magnitude less voluminous than andesites/dacites and rhyolites respectively (Wilson et al., 1995). Basalts of the TVZ are classified as high-alumina and are generated by a combination of rift-induced decompression melting and fluid-induced flux melting (Hiess et al., 2007; Law et al., 2021). Active calderas have high inputs of basalt from the mantle wedge, which is caused by fluid-fluxed melting of fertile mantle, i.e. mantle that has not undergone much previous melting (Barker et al., 2020; Zellmer et al., 2020). The mantle source is lherzolitic, as the sub-continental lithospheric mantle found further south in the TVZ has been removed by rifting and crustal thinning, causing the shift to rhyolitic rather than andesitic volcanism (Law et al., 2021). Regions without active calderas have lower inputs of basalt due to either a subdued influence from fluid-fluxing or a more depleted mantle source (Barker et al., 2020; Zellmer et al., 2020). In the latter mechanism, the depleted source is caused by prior melt extraction associated with caldera formation in the region, but these calderas are no longer active (Zellmer et al., 2020). Basaltic eruptions throughout the TVZ are often associated with faults and commonly erupt in association with rhyolitic magmas (Cole, 1970a; Hiess et al., 2007; Nairn and Cole, 1981). Basaltic volcanism exhibits a wide range of eruption style, both within and between individual eruptions and volcanic centres, and shallow conduit processes (including interaction with external, non-magmatic water) are thought to play a major role in determining eruption style (e.g., Carey et al., 2007; Houghton and Hackett, 1984).

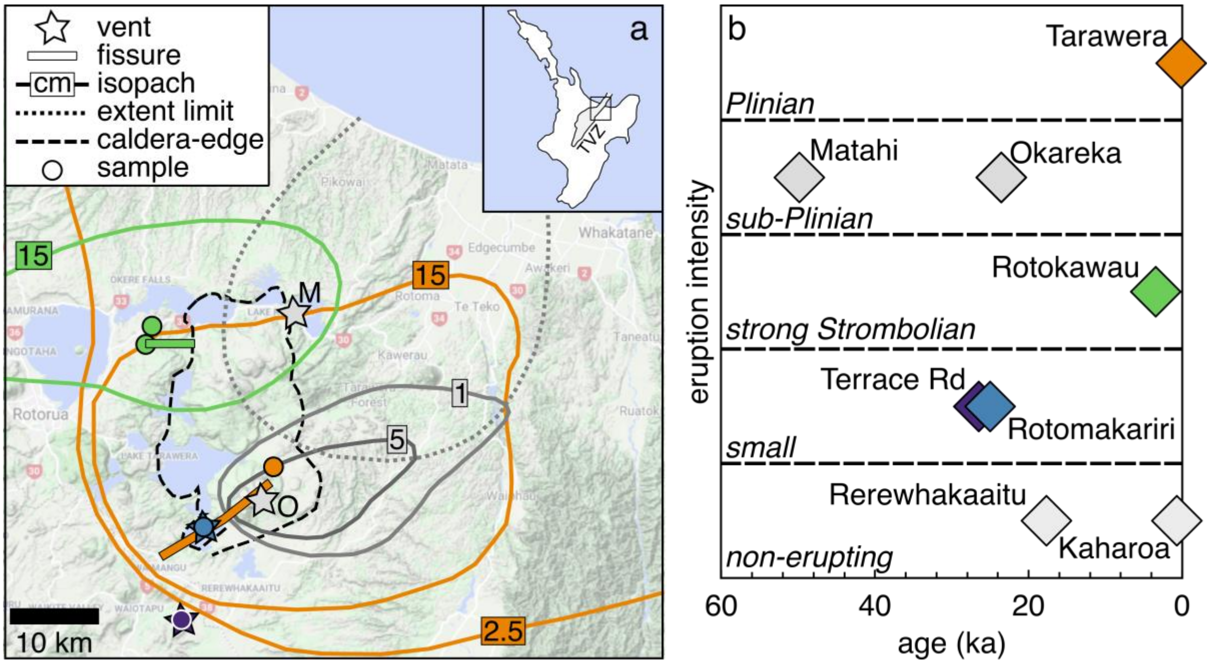

Figure 1 **(a)** Map of the region surrounding the Ōkataina Volcanic Centre (ŌVC), showing the caldera boundary; location of eruptive vents and fissures (Beanland, 1989; Burt et al., 1998; Darragh et al., 2006; Nairn, 2002, 1992); deposit thickness isopleths or extent limit (Beanland, 1989; Darragh et al., 2006; Nairn, 1992; Pullar and Nairn, 1972); and sample locations for this study for the basaltic eruptions (colours shown in (b) – eruptions analysed in this study are in colour and other basalts from around the ŌVC are shown in grey). Inset shows the location of the main map and the Taupō Volcanic Zone (TVZ, shaded area) in the North Island of Aotearoa New Zealand. M = Matahi, where the dotted-grey line is the extent limit; and O = Okareka, where the solid-grey lines are the 1 and 5 cm isopachs. **(b)** Qualitative eruption intensity against age (Buck et al., 2003; Hogg et al., 2003; Hopkins et al., 2021; Nairn, 2002; Newnham et al., 2003; Peti et al., 2021) for ŌVC basaltic magmas – Rerewhakaaitu and Kaharoa do not appear in (a) because they only occur as basaltic enclaves and blebs within a rhyolitic eruption.

The currently active ŌVC is overwhelmingly rhyolitic, but a diverse range of styles and intensities of basaltic explosive activity is also present within and outside the caldera boundary (Cole et al., 2014; Nairn, 2002) (Figure 1a). Since ~55 ka there have been at least six basaltic eruptions (and additionally two examples of mafic enclaves and blebs in exclusively rhyolitic eruptions) in this region, ranging from phreatomagmatic to magmatic and Strombolian to Plinian in intensity (Table 1 and Figure 1) (Cole et al., 2014; Nairn, 2002). Basaltic Plinian eruptions are rare in the geological record, and Tarawera is the one of the most recent (Cole, 1970a; Nairn, 1979; Rowe et al., 2021; Thomas, 1888; Walker et al., 1984).

Basaltic eruptions around the ŌVC are fed by dikes. Vents are often aligned along the main tectonic fabric (i.e., with a strike trending NE-SW), predominantly located on the Tarawera Linear Vent Zone, but are also found just outside the caldera boundaries (Nairn, 2002) (Figure 1a). Most individual eruptions issued from a single vent, but the Tarawera and Rotokawau eruptions occurred along fissures, displaying a range of style and intensity both spatially and temporally within each eruption (Nairn, 2002). For instance, the Tarawera eruption generated a ~17 km NE-SW fissure, with Strombolian to Plinian magmatic eruptions in the NE and phreatomagmatic eruptions in the SW where it intersected an active hydrothermal system (Nairn, 1979; Nairn and Cole, 1981; Rowe et al., 2021; Walker et al., 1984). The Tarawera fissure is broadly aligned with the TVZ extension direction, which contrasts markedly to the Rotokawau eruption where the fissure strikes E-W (Beanland, 1989). Additionally, many of the ŌVC rhyolitic eruptions are likely triggered by the injection of basaltic magmas (e.g., Leonard et al., 2002; Shane et al., 2008, 2007). Some rhyolitic eruptions were preceded by basaltic eruptions, with either no (e.g., Matahi prior to Rotoiti) or direct (e.g., mixed basaltic-rhyolitic clasts in Okareka) evidence for magma mixing prior to eruption, whereas others (e.g., Rerewhakaaitu and Kaharoa) host basaltic blebs and enclaves (e.g., Burt et al., 1998; Cole, 1973a; Cole et al., 2014; Leonard et al., 2002; Nairn, 1992; Pullar and Nairn, 1972; Schmitz and Smith, 2004; Shane et al., 2007, 2008a). The ŌVC is passively degassing CO_2 and heat today, and inferred basaltic dike events also occur (e.g., Benson et al., 2021; Hughes et al., 2019b; Mazot et al., 2014).

Table 1 Basaltic eruptions and magmas from around the Ōkataina Volcanic Centre (ŌVC) since the last caldera-forming eruption.

Eruption	Age (ka)	Description	DRE volume (km^3) [Column height (km)]
Tarawera*	1886 C.E.	Phreatomagmatic to magmatic, Strombolian to Plinian fissure[1–3]	0.25–0.48[4] [~28][3]
Kaharoa	0.6[5–6]	Enclaves in rhyolitic eruption[7–9]	>0.01[9]
Rotokawau*	3.44 ± 0.07[10]	Phreatomagmatic (Surtseyan) and Strombolian fissure[10–12]	0.55[11] [4.5–7][11]
Rerewhakaaitu	17.6[13]	Blebs in rhyolitic eruption[14]	n.d.
Okareka	23.5[15]	Single vent, sub-Plinian phase prior to rhyolitic eruption[16–17]	0.01[16,18]
Rotomakariri*	22–28[10]	Single vent tuff cone[10]	n.d.
Terrace Rd*	25–28, 28 ± 2[10]	Single vent (?), small phreatomagmatic[10]	n.d.
Matahi†	~45–55[19]	Single vent, sub-Plinian[20]	<1[21]

Notes: *Eruptions analysed in this study. †The Matahi eruption occurred just prior to the Rotoiti Ignimbrite that was the most recent ŌVC caldera-forming eruption. Volumes (DRE = dense rock equivalent) for Terrace Rd and Rotomakariri are not determined (n.d.), but are likely small due to their limited occurrence (Nairn, 2002). References: [1]Keam (1988), [2]Nairn and Cole (1981), [3]Walker et al. (1984), [4]Rowe et al. (2021), [5]Hogg et al. (2003), [6]Buck et al. (2003) [7]Leonard et al. (2002), [8]Nairn et al. (2001), [9]Nairn et al. (2004), [10]Nairn (2002), [11]Beanland (1989), [12]Beanland and Houghton (1978), [13]Newnham et al. (2003), [14]Shane et al., (2007), [15]Peti et al. (2021), [16]Darragh et al. (2006), [17]Nairn (1992), [18]Shane et al. (2008a), [19]see discussion in Hopkins et al. (2021), [20]Pullar and Nairn (1972), and [21]Froggatt and Lowe (1990).

All basalts (including blebs in rhyolitic eruptions) from around the ŌVC contain olivine, clinopyroxene, and plagioclase crystals (sometimes in aggregates) within a glassy (e.g., Matahi) to highly microcrystalline groundmass (e.g., Cole, 1970b; Law et al., 2021; Nairn, 2002, 1992; Rowe et al., 2021; Sable et al., 2009; Schmitz and Smith, 2004; Shane et al., 2008a). Additionally, most basalts contain xenocrystic quartz and rhyolitic material entrained during ascent (Beanland, 1989; Cole, 1973a; Nairn, 2002; Schmitz and Smith, 2004). Hornblende has only been observed in basaltic enclaves in the Kaharoa eruption in the ŌVC since ~55 ka (Leonard et al., 2002). Clast vesicularity ranges from dense to highly vesicular, even within an eruption (Beanland, 1989; Nairn, 2002; Shane et al., 2008a). Dense clasts are often used as evidence for interaction with external water leading to increased eruption intensity (e.g., Beanland and Houghton, 1978; Carey et al., 2007).

3 Methods

We sampled and analysed material from the Terrace Rd, Rotomakariri, Rotokawau, and Tarawera eruptions as they cover the full range of eruption styles and sizes (phreatomagmatic to magmatic and Strombolian to Plinian) observed around the ŌVC (Figure 1b). These eruptions occurred in an active caldera region, but Rotomakariri and Tarawera occurred inside the caldera boundary (along one of the main linear vent zones), whereas Terrace Rd and Rotokawau occurred outside the caldera boundary (Figure 1a). There are no published melt inclusion data for Terrace Rd, Rotomakariri, and Rotokawau, and only limited published data for Tarawera (Barker et al., 2020; Rowe et al., 2021); melt inclusions have been previously analysed from Okareka and Kaharoa (Barker et al. 2020).

Samples were collected during three fieldwork seasons between 2015 and 2017 (Figure 1a). Localities for deposits for the Terrace Rd, Rotomakariri, and Rotokawau eruptions were taken from Nairn (2002); exact sample locations and descriptions are given in Supplementary Material (including for Tarawera samples). For Tarawera, samples were collected off the volcano to avoid material that had cooled slowly, which can enhance post-entrapment crystallisation of melt inclusions (e.g., Lloyd et al., 2013). Samples were dried in a low-temperature oven then sieved into 1 φ size fractions. The clast densities for -3 to -6 φ from Terrace Rd, -4 to -5 φ from Rotomakariri, -3 to -4 φ from Rotokawau, and -4 to -5 φ from Tarawera were measured using the method of Houghton and Wilson (1989). Vesicularity was calculated assuming rock density was equal to that of an anhydrous melt (assumed to approximate the glass density) with the composition of the average whole rock data from the literature (given in Supplementary Material), calculated at room temperature and pressure using DensityX (Iacovino and Till, 2018). Two mean density samples were chosen to make thin sections from (random samples were selected for Rotokawau from a different location due to the small clast size sampled during our fieldwork).

To constrain pre-eruptive magmatic compositions, conditions, and processes for these eruptions, we analysed mineral and melt inclusion chemistry and textures. Scoria -2 to -3 φ in size were selected to ensure rapid clast cooling, thereby increasing the potential for glassy melt inclusions that had retained their initial volatile content (Lloyd et al., 2013). Olivine, pyroxene, and plagioclase crystals were hand-picked from gently crushed clasts and either bulk mounted in epoxy or individually mounted and polished to expose a melt inclusion at the surface. Both types of mounts were polished to ~1 μm using diamond-paste. Only naturally glassy melt inclusions were analysed; no rehomogenisation experiments were carried out.

Olivine, pyroxene, and plagioclase mineral separates were analysed using electron probe micro-analysis (EPMA) wavelength dispersive spectrometry (WDS). Unless otherwise stated, all analyses were taken from crystal cores. Melt inclusions from all eruptions were analysed using EPMA-WDS for major, minor, and volatile (S, Cl, and F) elements and for H_2O using calibrated volatiles-by-difference (Hughes et al., 2019a). A subset of melt inclusions from Tarawera was analysed for H_2O and CO_2 using secondary ion mass spectrometry (SIMS) prior to EPMA. To put mineral separate data into context, textural observations on thin sections were made using optical microscopy and scanning electron microscopy (SEM). Some mineral phases (and the groundmass glass for Rotomakariri) in the thin sections were analysed using semi-quantitative (sq) SEM energy dispersive spectroscopy (EDS) (sq-SEM-EDS) and EPMA-WDS to correlate the textures with mineral separates data.

We compiled mineral, melt inclusion, and whole rock data from the literature, particularly from basaltic eruptions not analysed in this study (e.g., Matahi, Okareka, Rerewhakaaitu, and Kaharoa), to expand upon our dataset. Several thermometers (melt, olivine-melt, clinopyroxene-melt, and clinopyroxene-orthopyroxene; Putirka, 2008), oxybarometers (melt

Fe^{3+}/Fe_T; Kress and Carmichael, 1991), and barometers (clinopyroxene-melt; Neave and Putirka, 2017, and H_2O-CO_2 melt concentrations; Mangan et al., 2021), as well as modelling using rhyolite-MELTS (Ghiorso and Gualda, 2015; Gualda et al., 2012), were applied to mineral, melt inclusion, and whole rock data from this study and the literature. Data collection and reporting for melt inclusions broadly follows the guidelines of Rose-Koga et al. (2021). Full analytical and calculation details, as well as all data collected and compiled, are provided in Supplementary Material.

4 Textural and chemical characteristics

Texturally and chemically, Tarawera, Rotokawau, and Terrace Rd scoria are more similar to each other than to scoria from Rotomakariri.

4.1 Vesicles, groundmass, and macrocrysts

Tarawera, Rotokawau, and Terrace Rd are characterised by vesicles with complex shapes in a highly crypto- to microcrystalline groundmass containing olivine, clinopyroxene, plagioclase, and Fe-Ti oxide microlites (Figure 2a, c, and d). Although the size and proportions of the microlites vary slightly between these eruptions, the main difference is that Tarawera is much more microcrystalline than Rotokawau and Terrace Rd (i.e., >90 groundmass area% of scoria at Tarawera). Rotokawau and Tarawera scoria are homogeneously brown-to-black, whereas Terrace Rd is highly variable in colour (black to light-brown), including small domains (<3 mm across) of black and grey material. At Terrace Rd, the groundmass is very similar in both the brown and black areas, although plagioclase microlites are slightly shorter in the black material. When in contact, microlites in the brown groundmass are flow-aligned around the edge, whilst the margins of the black groundmass are crenulated and wavy. Rotokawau also shows multiple groundmass textures, including flow alignment (Figure 2c). Rotomakariri scoria are homogeneously brown-to-black and have rounded vesicles in a groundmass of glass containing sparse microlites of plagioclase and clinopyroxene (Figure 2b). Further details are in the Supplementary Material.

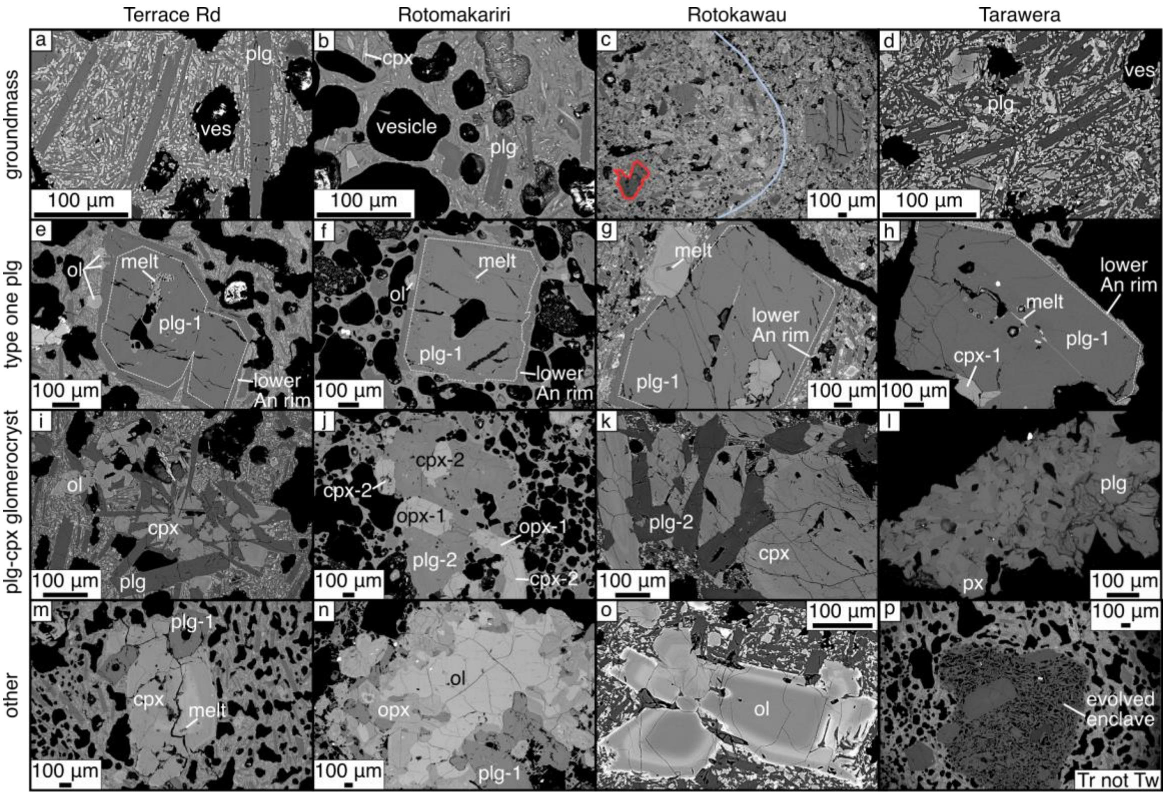

Figure 2 Annotated back-scattered electron (BSE) scanning electron microscope (SEM) images of scoria textures. Each column is a separate eruption: Terrace Rd (a, e, i, m, and additionally p at the bottom of the far-right column), Rotomakariri (b, f, j, n), Rotokawau (c, g, k, and o), and Tarawera (d, h, l). Different features are shown by row. **(a–d)** Groundmass textures, where in **(b)** plagioclase is An_{76}, and **(c)** shows alignment of plagioclase from basalt-basalt magma mixing (blue line) and a region of evolved material is outlined in red. **(e–h)** Group one plagioclase with high An cores ($An_{93–96}$) and lower An rims ($An_{76–87}$) forms glomerocrysts with other phases. **(i–m)** Glomerocrysts of plagioclase and pyroxene: **(i)** plagioclase, clinopyroxene, and altered olivine on the edge; **(j)** glomerocryst with group two plagioclase (core An_{83}, rim An_{79}), group two clinopyroxene (Mg# 75–78), and group one orthopyroxene (Mg# = 71 core, 75 rim); **(k)** group one clinopyroxene (Mg# 85) and group two plagioclase (An_{88}); **(l)** intergrown plagioclase and pyroxene; **(m)** group one plagioclase and olivine grains (Fo_{76}) attached to a group two clinopyroxene (Mg# = 65 core, 80 middle, 73 rim). **(n–p)** Other textures: **(n)** glomerocryst: centre is a partially resorbed olivine (Fo_{83}), with overgrowths of group one orthopyroxene (Mg# 76), group one and two plagioclase (An_{92} core, An_{85} rim), and some clinopyroxene on the outer portion; **(o)** olivine macrocryst (dark portions Fo_{80}, bright band Fo_{75}); and **(p)** evolved enclave (from Terrace Rd) containing group three plagioclase and quartz, with some evidence of reaction with basaltic melt at the margins. *Abbreviations:* ves = vesicle, ol = olivine, plg = plagioclase, cpx = clinopyroxene, opx = orthopyroxene, and px = pyroxene. White bar in bottom left of each image is 100 µm in length.

Terrace Rd, Rotokawau, and Rotomakariri contain abundant macrocrysts, mostly as glomerocrysts (Figure 2i–n), whereas Tarawera is almost macrocryst- and glomerocryst-free (see also Law et al., 2021). All eruptions have a similar mineralogy of olivine, plagioclase, and clinopyroxene, with Rotomakariri additionally containing abundant orthopyroxene. Alkali feldspars and quartz were found in all eruptions. Multiple groups of mineral compositions are observed across eruptions, which are outlined in Table 2. Olivine composition varies between eruptions, with a narrow range in forsterite (Fo) content at Terrace Rd and Tarawera and a wide range at Rotomakariri and Rotokawau (Figure 3a–e). Our data support the findings of Law et al. (2021), where olivines from Terrace Rd, Tarawera, and Rotokawau are group 1 and those from Rotomakariri are group 2 (Table 2). Groundmass olivine from Tarawera analysed by Rowe et al. (2021) has lower Fo than the macrocrystals (Figure 3a). Two groups of clinopyroxene are found in all eruptions: group one has high Mg#, whereas group two has low Mg# (Table 2 and Figure 3f–k). Group two includes the Tarawera groundmass clinopyroxene reported by Rowe et al. (2021). Orthopyroxene is common only in Rotomakariri, occurring as two groups (Figure 3h). Group one (high Mg#) is found as macrocrysts in Rotomakariri (and rarely Rotokawau and Tarawera) and sometimes as inclusions in lower Mg# clinopyroxene grains at Terrace Rd and Rotokawau. Group two (low Mg#), sometimes contains inclusions of apatite, and occurs in all eruptions. Plagioclase is present in three groups (Table 2 and Figure 3k–o). Group one cores are very calcic (>An_{90}) with coarse sieving and normal zoning to a thin, unsieved, less calcic rim. Group two plagioclase have lower An, are mostly unzoned and occur as both macrocrysts and inclusions in clinopyroxene at Terrace Rd, in low Mg# orthopyroxene at Rotokawau, and in both clinopyroxene and orthopyroxene at Rotomakariri. This plagioclase composition is similar to rims on group one plagioclase and plagioclase microlites in the Tarawera groundmass (Rowe et al., 2021). For both group one and two plagioclase FeO content is high and decreases with increasing An. Group three plagioclases are low in An and FeO, and texturally variable. Unlike mineral groups, which are shared across different eruptions, glomerocryst types are unique to individual eruptions. More detailed descriptions of both the mineral groups and glomerocryst types are provided in the Supplementary Material.

Table 2 Chemical characteristics of different mineral groups.

Mineral	Parameter	Group 1	Group 2	Group 3
Olivine	Fo	<86	72–88	
	NiO (wt%)	<0.2	<0.15	
	CaO (wt%)	>0.18	<0.07	
Clinopyroxene	Mg#	83–87	67–83	
Orthopyroxene	Mg#	65–80	46–57	
Plagioclase	An	>90	55–90	<55
	FeO_T (wt%)	>0.4	>0.4	<0.4

Notes: Blank space indicates textural type not present.

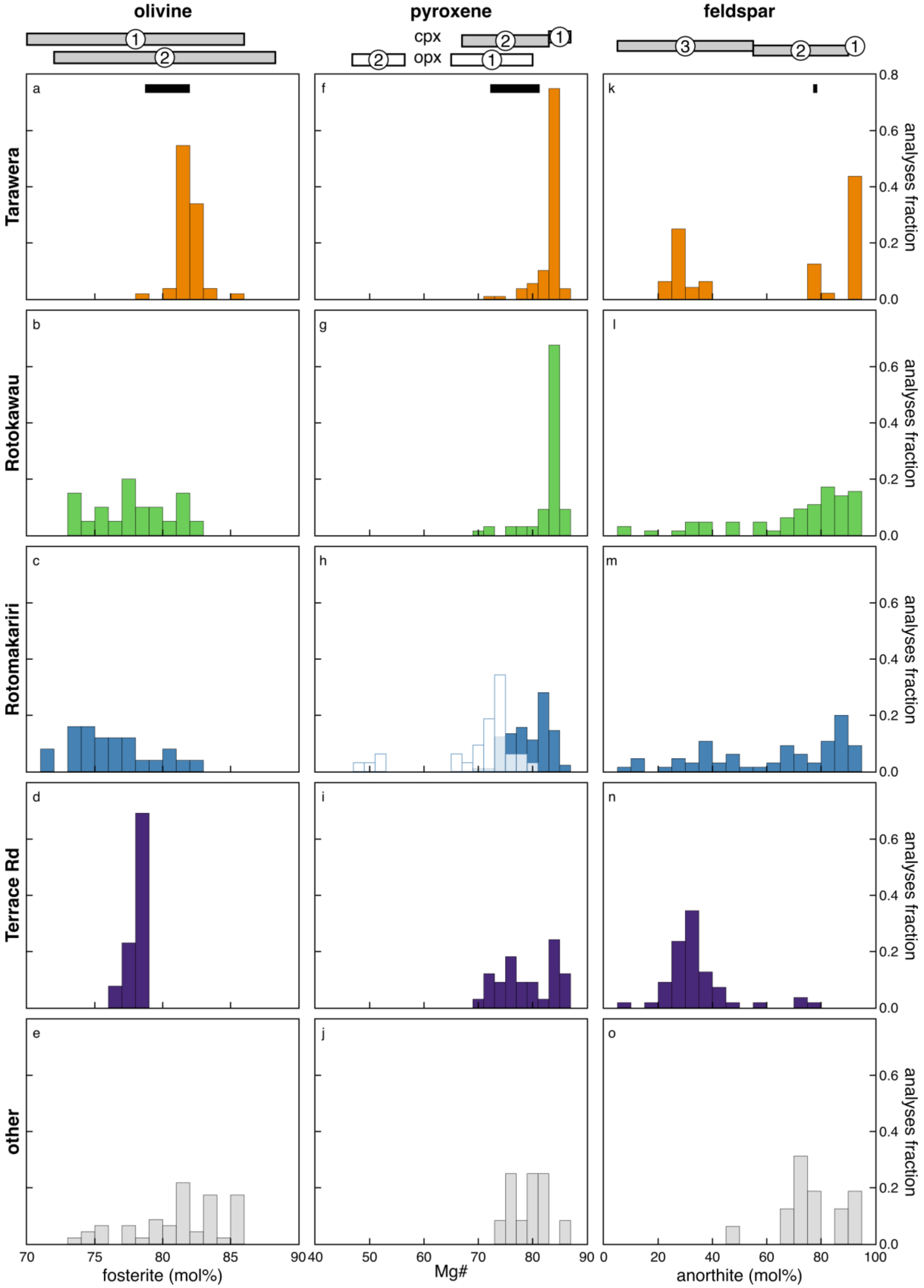

Figure 3 Histograms of mineral chemistry showing fraction of crystal core analyses in each compositional bin. Each column represents a different mineral phase, labelled along the top: **(a–e)** olivine – forsterite content, **(f–j)** pyroxene – Mg# (histograms are for cpx, except unfilled bars in **(h)** that are for opx), and **(k–o)** plagioclase – anorthite content. Each row represents an

individual eruption, which are labelled down the left-hand side and shown using colour: **(a, f, k)** Tarawera, **(b, g, l)** Rotokawau, **(c, h, m)** Rotomakariri, **(d, i, n)** Terrace Rd, and **(e, j, o)** other ŌVC basalts, which includes Kaharoa, Rerewhakaaitu, Okareka, and Matahi. Range of microlite compositions from Rowe et al. (2021) for Tarawera shown as black bars in (b, g, l). Different mineral groups described in the text indicated above panels: **(a)** for olivine (1 and two in grey), **(f)** for clinopyroxene (1 and 2 in grey) and orthopyroxene (1 and 2 in white), and **(l)** for plagioclase (1, 2, and 3 in grey). *Data sources:* Matahi (Davis, 1985); Terrace Rd (Law et al., 2021; this study); Rotomakariri (Law et al., 2021; this study); Okareka (Barker et al., 2020; Shane et al., 2008a); Rerewhakaaitu (Shane et al., 2007), Rotokawau (Beanland, 1989; Hiess et al., 2007; Law et al., 2021; this study); Kaharoa (Barker et al., 2020; Leonard et al., 2002), Tarawera (Barker et al., 2020; Hiess et al., 2007; Law et al., 2021; Rowe et al., 2021; this study). Additional figures are shown in Supplementary Material.

4.2 Melt inclusions

The vast majority of glass analyses in this study come from melt inclusions hosted in clinopyroxene, with minor olivine-, plagioclase-, and orthopyroxene-hosted melt inclusion and groundmass glass analyses (Figure 4 and Figure 5; additional data are shown in Supplementary Material). The Tarawera dataset is supplemented with melt inclusion data from Barker et al. (2020) and Rowe et al. (2021). Melt inclusions show considerable range in composition. Terrace Rd, Rotokawau, and Tarawera melt inclusions are predominantly basaltic to basaltic-andesite in composition, whereas Rotomakariri glasses are entirely andesitic (Figure 4).

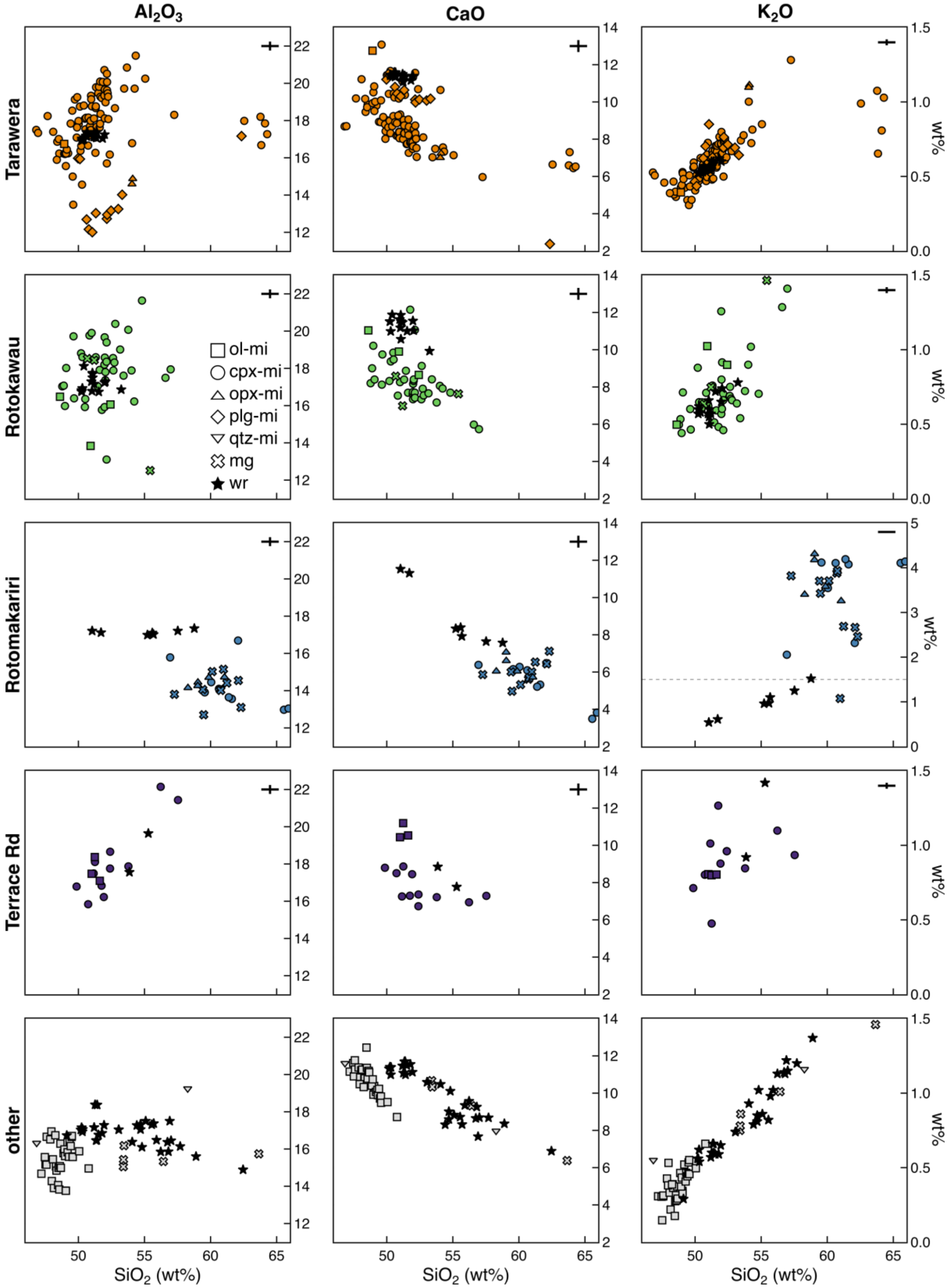

Figure 4 Melt composition data for Al_2O_3, CaO, and K_2O against SiO_2. Symbol shapes distinguish between melt inclusion (hosted in olivine, clinopyroxene, plagioclase, orthopyroxene, or quartz), groundmass glass, or whole rock analyses. Each row is for a different eruption(s), also indicated by symbol colour. Uncertainties for our data are indicated in the top-right corner of each panel and are two standard deviations of the precision based on

repeat analyses of VG-2 over all analytical sessions. Melt inclusion data are raw analyses (i.e., no corrections for post-entrapment processes), except Kaharoa, Okareka and three olivine-hosted Tarawera melt inclusions that were homogenised prior to measurement by Barker et al. (2020). K_2O data for Rotomakariri have a different y-axis scale: the dashed vertical line indicates the range shown for other eruptions for comparison. *Data sources:* melt inclusion and groundmass glass for Terrace Road, Rotomakariri, and Rotokawau (this study); Tarawera melt inclusions hosted in clinopyroxene and plagioclase (this study; Rowe et al., 2021), olivine (Barker et al., 2020), orthopyroxene and quartz (Rowe et al., 2021); olivine-hosted melt inclusions for Okareka and Kaharoa (Barker et al., 2020); glass analyses from mafic blebs from Rerewhakaaitu (Shane et al., 2007); ŌVC basaltic whole rock (Beanland, 1989; Bowyer, 2001; Cole, 1979, 1973b; Gamble et al., 1993, 1990; Grange, 1937; Hiess et al., 2007; Leonard et al., 2002; Nairn, 1992, 1981, 1979; Nairn et al., 2004; Nairn, 2002; Pittari et al., 2016; Rooney and Deering, 2014; Rowe et al., 2021; Schmitz and Smith, 2004; Shane et al., 2008a; Zellmer et al., 2020).

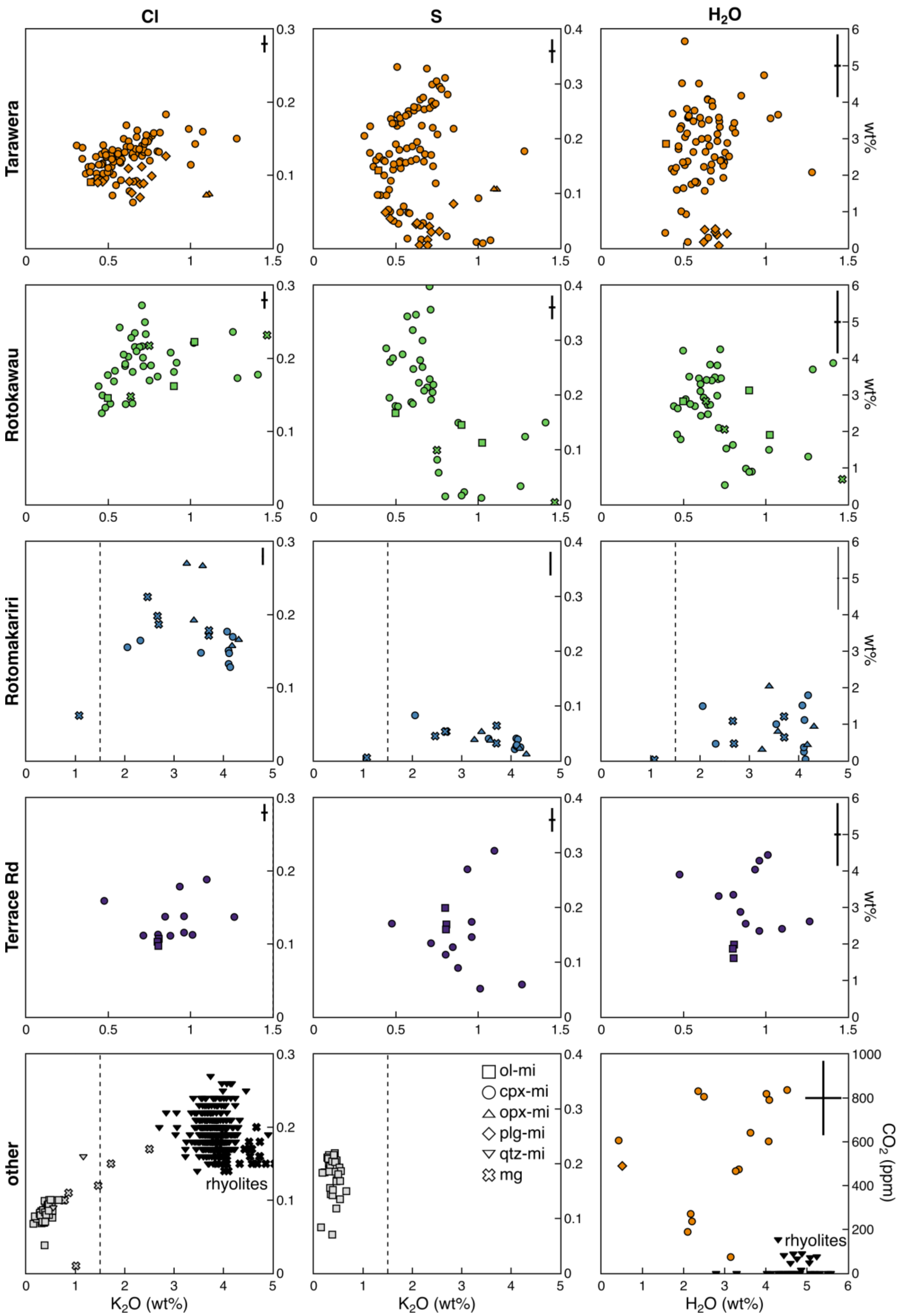

Figure 5 Melt composition data for Cl, S, and H_2O against K_2O. Symbol shape distinguishes between analyses of melt inclusions (hosted in olivine, clinopyroxene, plagioclase,

orthopyroxene, or quartz), groundmass glasses, and whole rocks. Each row is for a different eruption(s), also indicated by symbol colour. Uncertainties for our data are indicated in the top-right corner of each panel as two standard deviations of precision based on repeat analyses of VG-2 over all analytical sessions. Melt inclusion data are raw analyses (i.e., no corrections for post-entrapment processes), except Kaharoa (basalt), Okareka and three olivine-hosted Tarawera melt inclusions that were homogenised prior to measurement by Barker et al. (2020). K_2O for Rotomakariri and other eruptions have a different y-axis scale: the dashed vertical line indicates the range shown for other eruptions for comparison. The H_2O-CO_2 panel in the bottom-right is for Tarawera only, collected using SIMS (two H_2O data are from EPMA), where uncertainties are two standard deviations of the minimum precision based on repeat analyses of standards over all analytical sessions. *Data sources:* melt inclusion and groundmass glass for Terrace Road, Rotomakariri, and Rotokawau (this study); Tarawera melt inclusions hosted in clinopyroxene and plagioclase (this study; Rowe et al., 2021), olivine (Barker et al., 2020), orthopyroxene and quartz (Rowe et al., 2021); olivine-hosted melt inclusions for Okareka and Kaharoa (Barker et al., 2020); glass analyses from mafic blebs from Rerewhakaaitu (Shane et al., 2007); melt inclusions and groundmass glass from ŌVC rhyolites (Johnson et al., 2011); and ŌVC basaltic whole rock (Beanland, 1989; Bowyer, 2001; Cole, 1979, 1973b; Gamble et al., 1993, 1990; Grange, 1937; Hiess et al., 2007; Leonard et al., 2002; Nairn, 1992, 1981, 1979; Nairn et al., 2004; Nairn, 2002; Pittari et al., 2016; Rooney and Deering, 2014; Rowe et al., 2021; Schmitz and Smith, 2004; Shane et al., 2008a; Zellmer et al., 2020).

Crystallisation, diffusion, and bubble-formation can alter major and volatile element chemistry of melt inclusions after entrapment (e.g., Barth et al., 2019; Barth and Plank, 2021; Bucholz et al., 2013; Danyushevsky et al., 2000, 1988; Dungan and Rhodes, 1978; Gaetani et al., 2012; Gaetani and Watson, 2002, 2000; Hartley et al., 2014, 2015; Lowenstern, 2003, 1995; Moore et al., 2015; Nielsen et al., 1998; Rasmussen et al., 2020; Roedder, 1979; Saper and Stolper, 2020; Schiano, 2003; Sobolev and Shimizu, 1993; Wallace et al., 2015). On the basis of mineral-melt exchange equilibria, most melt inclusions were not in equilibrium with their host crystal, except three clinopyroxene- and six plagioclase-hosted melt inclusions. This indicates some post-entrapment crystallisation has occurred. The effect of post-entrapment crystallisation on major, minor, and volatile element trends was evaluated by adding back the composition of the host mineral until equilibrium between the calculated melt composition and host mineral composition was achieved (further details provided in Supplementary Material). The mean/maximum post-entrapment crystallisation correction (excluding plagioclase-hosted melt inclusions) are 6/23 % for Tarawera, 5/14 % for Terrace Rd, 3/9 % for Rotomakariri, and 4/28 % for Rotokawau. Although Fe-Mg diffusion may also be important, it is not possible to evaluate its effect on the clinopyroxene-hosted melt inclusions currently; for this reason, we focus on trends in oxides other than MgO and FeO.

Even when assuming the maximum degree of post-entrapment crystallisation (without Mg-Fe diffusion) for each clinopyroxene-, orthopyroxene-, and olivine-hosted melt inclusion, *trends* in major and volatile element chemistry do not change from those observed using the raw data (details in Supplementary Material). For instance, the positive correlation between SiO_2 and Al_2O_3 and K_2O, and negative correlation between SiO_2 and CaO are robust. Moreover, Rotomakariri melt inclusions remain much more evolved than the other melt inclusions. Hence, these trends reflect pre-entrapment processes for major elements. For this reason, uncorrected (i.e., raw) melt inclusion compositions are used throughout, and we focus on SiO_2, Al_2O_3, CaO, and K_2O (Figure 4). The effect of 10 % crystallisation on plagioclase-hosted melt inclusions was modelled to see its effect on trends in melt inclusion chemistry. This showed that the low Al_2O_3 concentrations are likely due to post-entrapment effects, but the difference in CaO compared to clinopyroxene-hosted melt inclusions is likely a pre-entrapment feature (Figure 4).

Only the glass composition of melt inclusions was analysed; there was no attempt to account for volatiles contained in co-existing vapour bubbles (i.e., composition and size of vapour bubbles were not measured) to reconstruct bulk melt inclusion compositions. CO_2 is greatly affected by bubble formation, whilst H_2O, S, and Cl are less affected due to lower partitioning into the vapour phase and/or potential kinetic effects (e.g., Hartley et al., 2014; Maclennan, 2017; Moore et al., 2015; Rasmussen et al., 2020; Wallace et al., 2015). Rather than add additional uncertainty related to reconstructing the original melt composition, we assume CO_2 concentrations represent minimum estimates of the CO_2 content of the melt, and do not try and fit degassing trends to our data. Bulk (i.e., melt + bubble) H_2O content can additionally be altered by diffusion into or out of the melt inclusion (e.g., Barth et al., 2019; Barth and Plank, 2021; Bucholz et al., 2013; Gaetani et al., 2012; Hartley et al., 2015, 2014). The possibility of de/rehydration is considered for each eruption.

Basaltic to basaltic-andesite melt inclusions are similar in group one and group two clinopyroxenes and olivines from Terrace Rd, Rotokawau, and Tarawera, although olivine-hosted melt inclusions at Terrace Rd have higher CaO. There is no trend in melt composition with clinopyroxene Mg#, although the two Rotokawau melt inclusions hosted in $Mg\#_{76}$ clinopyroxene have the most evolved melt chemistry. At Rotokawau and Tarawera, melt inclusions have a wide range in H_2O content (0–5.5 wt%), whereas H_2O concentrations at Terrace Rd have a more limited range (2.2–4.8 wt% H_2O) (Figure 5). Terrace Rd and Tarawera have similar chlorine concentrations (1110–1880 and 630–1870 ppm Cl respectively) that are lower than Rotokawau (1250–2730 ppm Cl). Total sulphur (S_T) has a similarly wide range in all three eruptions (50–3980 ppm S_T) and fluorine concentrations are also similar (290–1100 ppm F). CO_2 (74–831 ppm) was measured for a subset of Tarawera melt inclusions only. Broadly, there is a positive correlation of K_2O with H_2O, S_T and Cl (Figure 5). At Rotokawau and Tarawera, there is a second population of melt inclusions with S_T <1000 ppm where H_2O and S_T (but not Cl) negatively correlate with K_2O. Tarawera melt inclusions hosted in group one plagioclase are basaltic with either the same (single grain) or lower Al_2O_3. They are volatile-poor in comparison to clinopyroxene-hosted melt inclusions, and K_2O negatively correlates with S_T and Cl (single grain from this study). The basaltic-andesite inclusions hosted in orthopyroxene have similar CaO, but different Al_2O_3, to clinopyroxene-hosted melt inclusions (Rowe et al., 2021).

Rotomakariri melt inclusions hosted in group two clinopyroxene and group one orthopyroxene and groundmass glass are mostly andesitic (two are dacitic), with low CaO and Al_2O_3 (Figure 4). H_2O and S_T are lower than most of the basaltic to basaltic-andesite melt inclusions, although similar to the low-sulfur (S_T <1000 ppm) set of clinopyroxene-hosted melt inclusions (Figure 5). Chlorine is high and similar to Rotokawau; fluorine is much higher than any of the basalts. At Tarawera, a few clinopyroxene-hosted melt inclusions are also andesite-dacite, but have higher Al_2O_3 and lower K_2O than Rotomakariri melt inclusions (Figure 4). A single andesite melt inclusion hosted in an Na-rich plagioclase from Tarawera has similar Al_2O_3 to the other Tarawera andesite-dacite melt inclusions, although its K_2O resembles Rotomakariri andesite melt inclusions. Rhyolitic melt inclusions and groundmass glass are associated with group two orthopyroxene and quartz from Rotokawau and Tarawera, and have very low S_T (0–70 ppm).

5 Pre- and syn-eruptive storage, evolution, and mixing of multiple magmas

The bulk magma (i.e., whole rock) composition erupted in basaltic eruptions (and found as basaltic enclaves in rhyolitic eruptions) from around the ŌVC is similar (Figure 4). However, the different compositional groups of clinopyroxene, orthopyroxene, and plagioclase, in combination with different melt inclusion compositions, indicate that multiple components are found across these basaltic eruptions (Figure 3 and Figure 4). Therefore, it is useful to group these components when discussing magmatic evolution during crustal storage. Based on the mineral and melt inclusion compositions there are five different components. There are two basalt to basaltic-andesite components found in all eruptions (Basalt-1 and Basalt-2); two andesite components that are much less common and more specific to the Rotomakariri (Rm) and Tarawera (Tw) eruptions (Andesite-Rm and Andesite-Tw); and a minor amount of rhyolite component found in all eruptions (Table 3). These components are repeatedly sampled as the groups of mineral types and melt inclusion compositions are common to many different eruptions. Similar melt inclusions (albeit more primitive) and mineral chemistries are found in other basalts from around the ŌVC (e.g., Kaharoa, Okareka, Matahi, and Matahina) and even in Taupō Volcanic Centre (TVC) basaltic material (e.g., Oraunui), showing that these are common features within the TVZ (Allan et al., 2017; Barker et al., 2020; Deering et al., 2011; Rooyakkers et al., 2018; Wilson et al., 2006). Each component may reflect differences in source (e.g., initial magma composition due to degree of slab influence), storage conditions (e.g., pressure, temperature, oxygen fugacity), processes (e.g., varying degrees of cooling- or decompression-induced crystallisation or crustal assimilation), physical state (mush-like in the crust, or solidified as an intrusion or after eruption at the surface) or combinations thereof. We use oxy-thermo-barometry (Figure 6), rhyolite-MELTS modelling (Figure 7), and comparison to experiments to explore the crystallisation conditions of Basalt-1, Basalt-2, and Andesite-Rm melts (calculation details are in Supplementary Material). As the same components occur in eruptions separated spatially and temporally, these sets of conditions must be common around the ŌVC even though magmas themselves were not sourced from the same spatio-temporal reservoir. The textures observed in each eruption reflect different processes during ascent, such as magma mixing and microlite crystallisation.

Table 3 Occurrence, mineralogy, conditions, and physical state for different components found in basalts from around the ŌVC.

Component	Occurrence	Mineralogy	Conditions	State
Basalt-1	All	ol-1, ol-2, cpx-1, plg-2	Deep (0.3–0.7 GPa), warm (1000–1200 °C), oxidised (ΔNNO=0 to +2), water-saturated	Mush
Basalt-2	All	plg-1	Primitive	
Andesite-Rm	Rare	cpx-2, opx-1	Shallow (~0.1 GPa), cool (~950 °C), reduced (ΔNNO-1 to 0)	Mush
Andesite-Tw	Rare		Cool (~850 °C)	
Rhyolite	All	opx-2, plg-3	Shallow (0.10–0.26 GPa) and cool (940–700 °C) with variable f_{O_2}	Solid

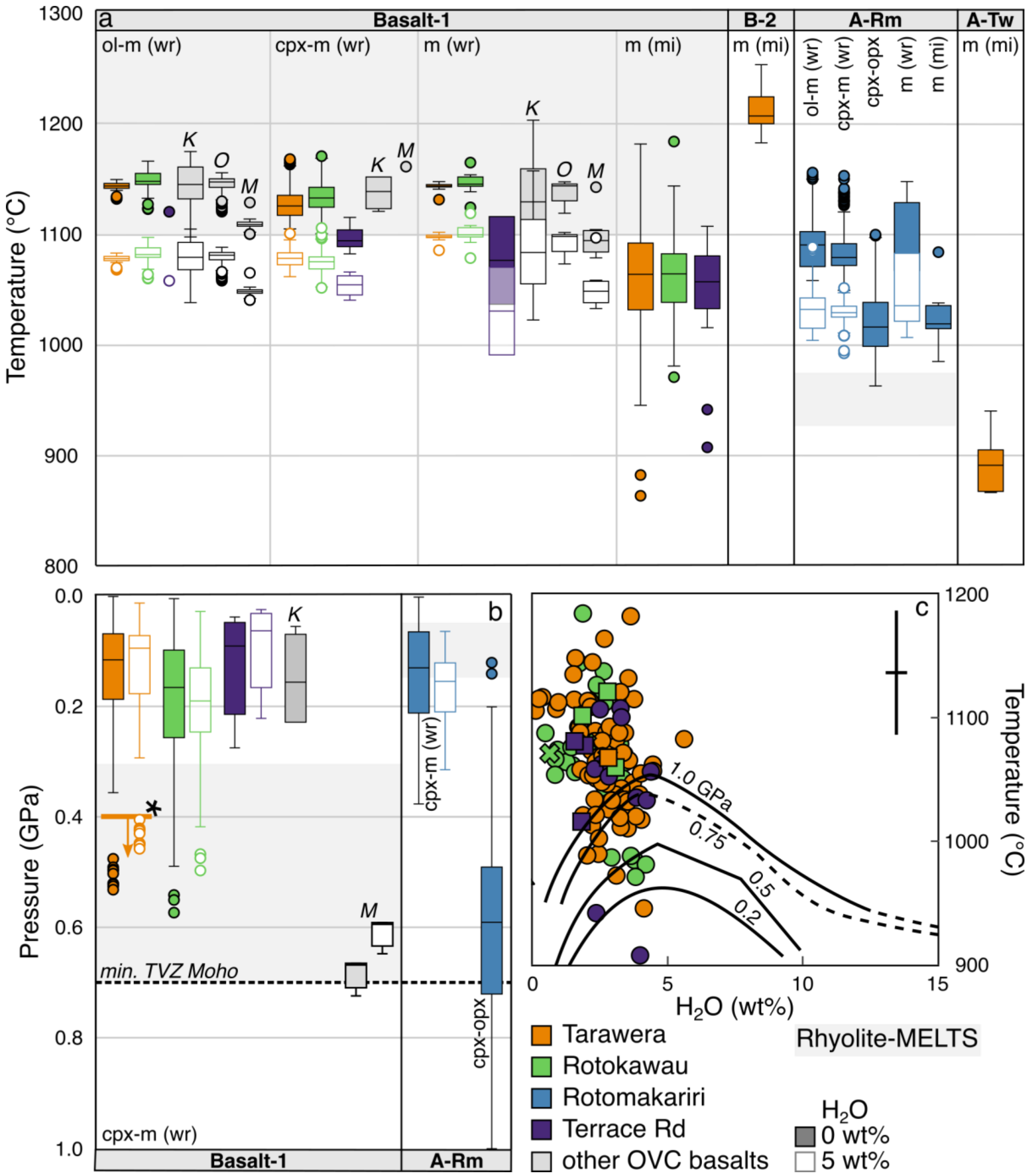

Figure 6 Box and whisker plots for **(a)** temperature and **(b)** pressure for each eruption (shown by colour, other ŌVC basalts include Kaharoa – *K*, Okareka – *O*, and Matahi – *M*) grouped by magma type in **bold** (along the top of (a) and the bottom of (b)) and then by thermobarometry method. The edges of the "box" are at the 1st and 3rd quartile of the data, with the median indicated by a horizontal line within the box. The "whiskers" extend out to the minimum and maximum data points within 1.5× the interquartile range (range between 1st and 2nd quartile) beyond the 1st and 3rd quartiles. Any outliers outside the whiskers are shown as individual data points (circles). The standard errors of estimate (SEE) are ±43–56 °C for thermometers and ±0.14 (cox-m) and ±0.32 (cpx-opx) GPa for barometers. Estimates using whole rock compositions are shown assuming a melt composition that is anhydrous (filled) or H_2O-saturated (≤5 wt%, unfilled); measured H_2O content is used for melt inclusions. A minimum pressure estimate for Tarawera using the highest H_2O-CO_2 melt measurement shown by

horizontal line (*) and a downwards pointing arrow. Ranges inferred from rhyolite-MELTS modelling shown as grey shaded regions. Minimum depth of the TVZ Moho (Bannister et al. (2004) indicated in (b) by dashed horizonal line. *Abbreviations*: ol = olivine, m = melt, wr = whole rock, cpx = clinopyroxene, mi = melt inclusion, opx = orthopyroxene, B-2 = Basalt-2, A-Rm = Andesite-Rm, and A-Tw = Andesite-Tw. Full descriptions of calculations given in Supplementary Material. **(c)** Temperature against H_2O content. Curves are maximum temperature amphibole is stable at for a given bulk H_2O content of the system from Foden and Green (1992) for different pressures (written on each line). Symbols (see Figure 4 for interpretation of the symbol shape) are melt inclusion data, where temperature is derived from the melt inclusion composition and measured H_2O concentration is plotted, which is a minimum for the system. Uncertainties are indicated for *T* (±1SEE) and H_2O (±2 sd of the precision based on repeat analyses of secondary standard VG2) in the top corner.

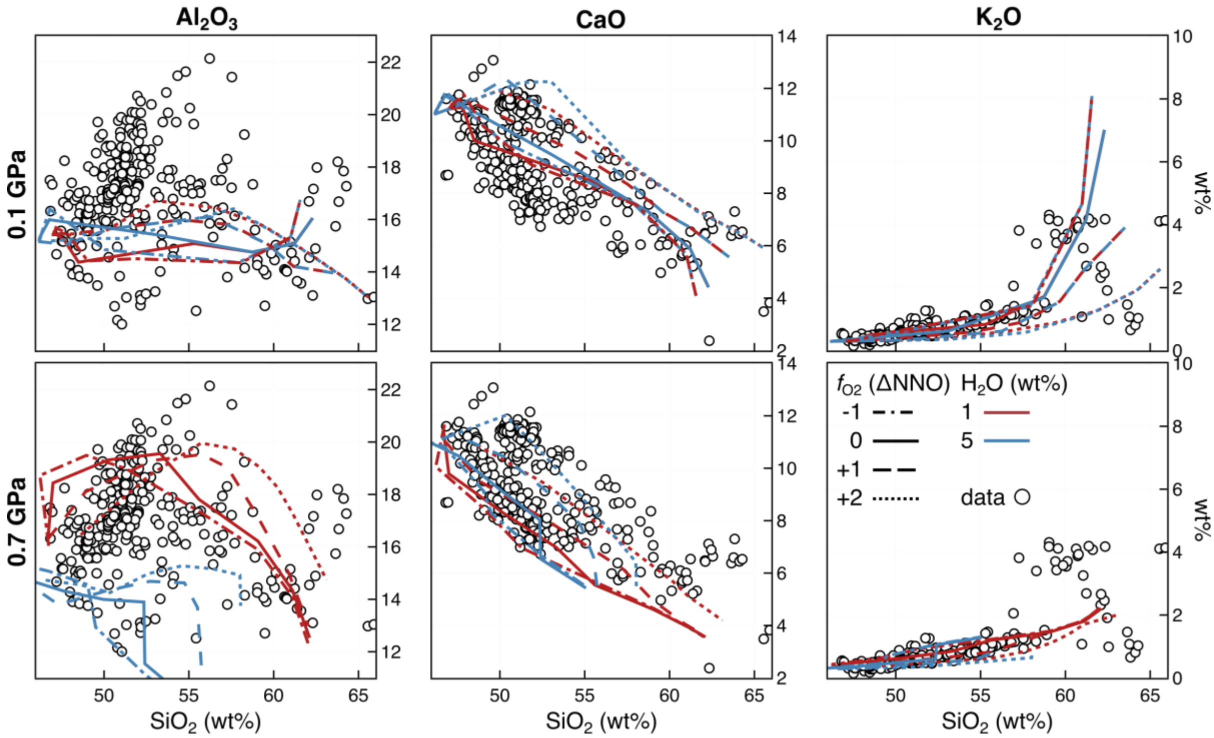

Figure 7 Rhyolite-MELTS modelling at 0.1 GPa (top row) and 0.7 GPa (bottom row) at low (1 wt%, red) and high (5 wt%, blue) H_2O and various oxygen fugacity (ΔNNO-1 dot-dash, 0 solid, +1 dash, and +2 dot) from a single melt composition. Melt inclusion and whole rock data shown as white circles. Additional results shown in Supplementary Material.

5.1 *Basalt-1*

Basalt-1 encompasses most of the mineral and melt inclusion analyses in this study, namely type one clinopyroxene, type two plagioclase, and their melt inclusions; and the groundmass material (except for Rotomakariri) (Figure 3 and Figure 4). Olivine compositions show Basalt-1 melts are not mantle-derived, but have already undergone crystallisation deeper in the system (Law et al., 2021). Both group one and two olivines as defined by Law et al. (2021) could have been derived from Basalt-1, where group two olivines crystallised deeper in the system and are sourced from cumulates. Alternatively, group two olivines may derive from a separate basaltic melt.

The spread in temperatures inferred from thermometry (Figure 6a) suggests cooling-induced crystallisation is responsible for the compositional range of whole rock and melt inclusion data.

The narrower spread in compositions and temperatures for whole rock and minerals compared to melt inclusions is consistent with the basaltic bulk composition of the system. Conversely, melt inclusion compositions reflect local changes in temperature and associated crystallisation, recording the melt present in the primary mush system near the solidus. The mushy nature of storage is also evidenced by abundant glomerocrysts in Terrace Rd, Rotomakariri, and Rotokawau (Figure 2i–n). A wide range of pressures (~0.7 GPa to surface) is derived from melt-clinopyroxene barometry, with most estimates <0.3 GPa (Figure 6b). The highest H_2O-CO_2 measurements require some melts to be derived from at least 0.4 GPa (Figure 6b). These estimates overlap with pressure-temperature estimates for Tarawera from Rowe et al. (2021), and imply polybaric storage of basaltic magmas, especially given the large model errors associated with this barometer (±0.14 GPa; Putirka, 2008). The increase in Al_2O_3 with increasing SiO_2 requires plagioclase crystallisation to have been suppressed, suggesting differentiation at higher pressures (e.g., Blatter et al., 2013; Marxer et al., 2021; Müntener and Ulmer, 2018a; Nandedkar et al., 2014). The limited literature whole rock Fe^{3+}/Fe_T data imply relatively oxidised conditions (~ΔNNO+1). Rhyolite-MELTS modelling suggests the range in melt inclusion compositions can be derived by equilibrium crystallisation during cooling (to 1100 °C) from a single melt composition deeper than 0.3 GPa at relatively oxidised (ΔNNO=0 to +2) and H_2O-saturated conditions (Figure 7). Despite broadly similar melt chemistry between eruptions, the detailed mineral compositions (e.g., olivine and clinopyroxene, Figure 3) and glomerocryst textures are distinct (Figure 2i–n) indicating evolution in discrete, isolated pods prior to eruption, consistent with the temporal and spatial spread of eruptions.

Trends for H_2O and CO_2 are scattered, reflecting post-entrapment processes overprinting original magmatic conditions, such as bubble formation reducing CO_2 concentrations and H-diffusion modifying H_2O (e.g., Barth et al., 2019; Barth and Plank, 2021; Bucholz et al., 2013; Gaetani et al., 2012; Hartley et al., 2015, 2014; Maclennan, 2017; Moore et al., 2015; Rasmussen et al., 2020; Wallace et al., 2015) (Figure 5). The highest measured concentrations are ~5 wt% H_2O and ~800 ppm CO_2, reflecting lower bounds on the H_2O-CO_2 concentrations of the magma. The measured water contents overlap with inferred melt water contents from melt inclusions and clinopyroxene H contents from Rowe et al. (2021). Positive correlation of Al_2O_3 and SiO_2 in clinopyroxene-hosted melt inclusions, reaching up to ~22 wt% Al_2O_3, requires plagioclase-suppression during crystallisation, such that clinopyroxene (± olivine) crystallisation controls melt composition (Figure 4). Based on experimental data, attaining such high Al_2O_3 concentrations requires at least some crystallisation of an H_2O-rich magma at depth (e.g., Blatter et al., 2013; Müntener and Ulmer, 2018; Nandedkar et al., 2014). This is consistent with high H_2O contents (~5 wt%) measured in some melt inclusions and the high pressures from melt-clinopyroxene and melt H_2O-CO_2 barometry (Figure 6b). This would suggest these melts are derived from the high-degrees of fluid flux melting associated with caldera regions, as inferred by Barker et al. (2020) and Zellmer et al. (2020).

Amphibole was not observed in the eruptions studied here; it has been described only in the groundmass of basaltic and gabbroic enclaves from the Kaharoa eruption, where amphibole crystallisation is thought to have been triggered by a late-stage increase in H_2O, possibly due to interaction with rhyolite (Leonard et al., 2002). Most of the melt inclusions at Tarawera, Rotokawau, and Terrace Rd record temperatures that are too high (>1050 °C) for amphibole stability despite their relatively high H_2O concentrations (Figure 6c) (Foden and Green, 1992). This suggests that basalt-rhyolite mixing prior to the Kaharoa eruption moved the magma into the amphibole stability field by cooling, rather than by increasing its H_2O content.

The more primitive melt inclusions in this group have elevated volatile concentrations, reflecting the influence of a subducted slab component added to the mantle wedge source regions (e.g., Wysoczanski et al., 2006). The more evolved (but still basaltic-andesite) melt inclusions have even higher volatile concentrations, which are similar to (H_2O, Cl) or greatly exceed (CO_2, S_T) volatile concentrations in ŌVC rhyolites (e.g., Johnson et al., 2011). This supports the inference that basalts exchange volatiles with rhyolitic magmas during crustal interactions (e.g., Leonard et al., 2002; Shane et al., 2008a, 2008b, 2007). Additionally, Basalt-1 at Rotokawau has higher S_T and Cl concentrations compared to the other basaltic eruptions (Figure 5). For Tarawera and Rotokawau, melt inclusions can be divided into two sub-groups based on S_T concentrations above and below ~1000 ppm (Figure 5).

Sulphur concentrations in melt inclusions require two separate regimes of crystallisation as previously observed by Rowe et al. (2021). We suggest that these regimes correspond to isobaric cooling and decompression-induced degassing (Figure 5). Concentrations of S_T and Cl increase in the melt during crystallisation for melt inclusions with >1000 ppm S_T, indicating these elements behaved incompatibly (i.e., were not partitioned into coexisting solids or exsolved fluids) (Figure 5). The magma may either have been volatile-undersaturated, such that there was no fluid phase for Cl or S to partition into, or fluid-melt partition coefficients for S and Cl at these conditions were very low (e.g., Gennaro et al., 2021; O'Neill, 2020; Tattitch et al., 2021; Thomas and Wood, 2021). If the magma was initially fluid-undersaturated, this would contrast with most arc regions where high magmatic CO_2 concentrations result in fluid-saturation deep in the crust (e.g., Wallace, 2005). Rotokawau and Tarawera melt inclusions with <1000 ppm S_T show the same trend for chlorine but the opposite trend for sulfur (i.e., decreasing S_T with crystallisation, Figure 5). Decreasing pressure during ascent drives crystallisation and degassing, forming a fluid that sequesters S, but not Cl (e.g., Lesne et al., 2011). The melt initially contained ~1700 ppm S_T and ~700 ppm Cl (~1200 ppm Cl for Rotokawau), but the maximum concentrations are ~3000 ppm S_T and ~2000 ppm Cl (2800 ppm Cl for Rotokawau).

In summary, Basalt-1 is volatile-rich and evolved from a single, primitive, oxidised magma in distinct, isolated, mushy pods due primarily to cooling-induced crystallisation, with some additional degassing during ascent.

5.2 Basalt-2

Basalt-2 is represented primarily by group one plagioclase and its melt inclusions that are chemically distinct from Basalt-1 (Figure 3 and Figure 4). The low Al_2O_3 of Basalt-2 likely represents post-entrapment crystallisation on the walls of the inclusion. However, even considering the effects of post-entrapment crystallisation, these compositions do not overlap clinopyroxene-hosted melt inclusions associated with Basalt-1 (see Supplementary Material). The ubiquitous thin rims of type two plagioclase (part of Basalt-1) at the edge of type one plagioclases show that these two basalts are not in equilibrium (Figure 2e–h). Additionally, $^{87}Sr/^{86}Sr$ data for these high-An plagioclases are distinctly more radiogenic than the groundmass, supporting the suggestion that they are derived from a separate magma (Rowe et al., 2021). These plagioclase crystals are likely in equilibrium with the most primitive TVZ basalts (Wilson et al., 2006) as their composition are in equilibrium with primary melt compositions calculated by Zellmer et al. (2020), but not melt inclusions or average whole rock for each eruption (Figure 8; calculation details are given in the Supplementary Material).

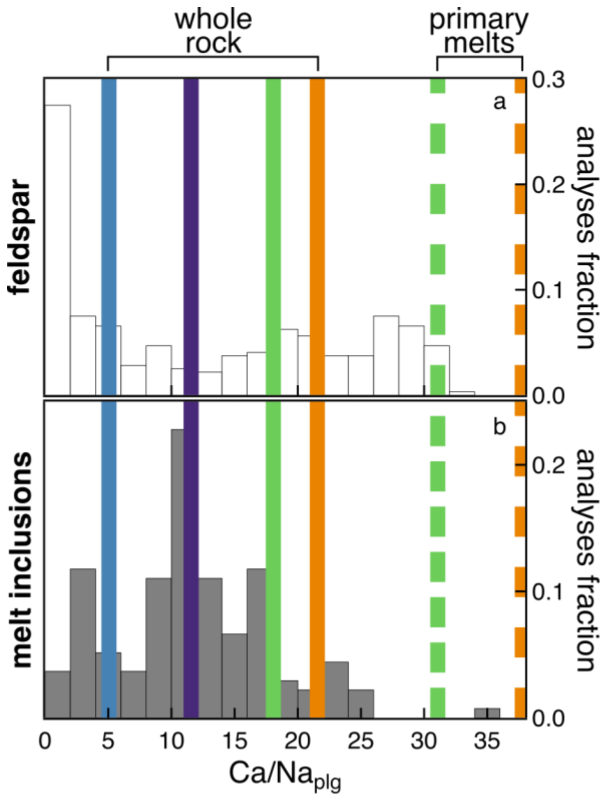

Figure 8 Ca/Na ratios in plagioclase: **(a)** from all analysed grains; and **(b)** calculated for equilibrium with melt inclusions from this study. Solid vertical lines are calculated Ca/Na$_{plg}$ in equilibrium with average whole rock data for each eruption, whereas dashed vertical lines are in equilibrium with primary melt compositions calculated by Zellmer et al. (2020) (Terrace Rd = purple, Rotomakariri = blue, Rotokawau = green, and Tarawera = orange).

High anorthite plagioclase (>An_{90}) can be indicative of hydrous conditions (e.g., Panjasawatwong et al., 1995; Takagi et al., 2005). The high magmatic water contents would occur as melting is driven by fluid-fluxing of a fertile mantle in active calderas (e.g., Barker et al., 2020; Zellmer et al., 2020). Plagioclase-liquid hygrometry using Waters and Lange (2015) suggests 5–7 wt% H_2O in the melt, yet the analysed melt inclusions are almost anhydrous (Figure 5). This suggests hydrogen loss from the melt inclusions via diffusion, either during storage in a low-H_2O melt or degassing during ascent (e.g., Hamada and Fujii, 2007). The higher temperatures compared to Basalt-1 (up to ~1250 °C) recorded by the melt inclusions would then reflect their low H_2O content due to dehydration (Figure 6a). Alternatively, the high anorthite content could be due to high Ca/Na in the melt and not reflect high water contents in the melt (e.g., Panjasawatwong et al., 1995). In this case, the low H_2O and high temperatures could be characteristics of the primary melt. Their occurrence as inclusions in clinopyroxene indicates plagioclase crystallisation before clinopyroxene, which occurs at lower H_2O. This may reflect the decompression melting source that is thought to dominate in intracaldera regions (Barker et al., 2020; Zellmer et al., 2020). Hence, decompression melting could also be a minor component of active calderas.

Group one plagioclase composition is not only found in basaltic material from around the ŌVC since ~55 ka, but also in basaltic material from the ~26.5 ka TVC Oruanui eruption (Allan et al., 2017; Rooyakkers et al., 2018; Wilson et al., 2006) and the ~330 ka ŌVC post-caldera deposits following the Matahina eruption (Deering et al., 2011). The ubiquity of group one plagioclase in spatially and temporally separated ŌVC (and TVC) basalts requires common crystallisation conditions. In summary, Basalt-2 is primitive and could either be hydrous and derived from fluid-flux mantle melting or dry and derived from decompression mantle melting. Further investigation is needed to unravel these processes.

5.3 Evolved magmas: Andesite-Rm, Andesite-Tw, and Rhyolite

Rotomakariri consists of mostly Andesite-Rm, containing group two clinopyroxene, group one orthopyroxene, their melt inclusions, and the groundmass material (Figure 3 and Figure 4). The occurrence of group two clinopyroxene in other eruptions suggests Andesite-Rm, although uncommon in the ŌVC, is not unique to Rotomakariri (Figure 3f–j). Two-pyroxene thermobarometry suggests high pressures (~0.6 ± 0.4 GPa, with large model uncertainties of ±0.32 GPa) and temperatures (~1000–1100 °C) (Figure 6b), This is unusually hot for an andesite. Rhyolite-MELTS modelling suggests Andesite-Rm can form from a similar initial magma composition as Basalt-1. However, equilibrium crystallisation is to a lower T (~950 °C), shallower (0.1 MPa, which contrasts markedly with the two-pyroxene barometry), and under more reducing conditions (ΔNNO-1 to 0) (Figure 7). Rotomakariri melt inclusion H_2O contents are very low, but this could indicate diffusive loss of H_2O, which is supported by many Rotomakariri melt inclusions being crystallised (these were not analysed). The low Cl and S_T concentrations indicates partitioning into a coexisting fluid. This is expected at low pressures and the hot, dry melt conditions observed; especially for sulphur in more evolved melt compositions (e.g., Clemente et al., 2004; Gennaro et al., 2021; O'Neill, 2020; Tattitch et al., 2021; Thomas and Wood, 2021) (Figure 5).

Andesite-Tw is chemically distinct from Andesite-Rm and melt inclusions record a lower temperature of ~850 °C (pressures could not be estimated from the available data, Figure 6a). As evidence for Andesite-Tw is only found in a few melt inclusions at Tarawera, it is not considered volumetrically important around the ŌVC (Figure 4). Rhyolite-MELTS modelling did not recreate this composition from the same initial magma composition used for Basalt-1 and Andesite-Rm.

A rhyolite component is found in all eruptions and is associated with type two orthopyroxene, type three plagioclase, quartz, alkali feldspars, and the rhyolitic melt inclusions (Figure 3 and Figure 4). It has a similar composition to ŌVC rhyolitic eruptions and is assumed to have evolved under similar conditions: pressures of 0.10–0.26 GPa from melt inclusion H_2O-CO_2 barometry, the presence of cummingtonite, and glass composition at or near to the quartz-albite-orthoclase-water ~0.2 GPa cotectic; and temperatures of 700–940 °C (narrower ranges are inferred for individual rhyolitic magma batches), mostly from Fe-Ti oxide thermometry and some from melt inclusion heating experiments (summarised in Cole et al., 2014; Smith et al., 2005). Textures suggest it was entrained when solid (i.e., solidified in the crust or erupted at the surface, then buried).

5.4 Similar storage conditions and volatiles prior to eruptions of varying style

Basalt-1 is the main magma type present in basaltic eruptions around the ŌVC. It comprises most of the material at Tarawera, Rotokawau, and Terrace Rd, and this is also likely the case for Okareka and Matahi and the basaltic material from Kaharoa and Rerewhakaaitu (Figure 3 and Figure 4). Rotomakariri is an exception and is therefore excluded from the following discussion: it does contain Basalt-1 material but is mostly composed of Andesite-Rm (Figure 3 and Figure 4). Temperature estimates using various thermometers based on whole rock and melt inclusion compositions from the different eruptions and Rhyolite-MELTS modelling overlap, especially given model uncertainties (~1150 °C anhydrous or ~1090 °C assuming 5 wt% H_2O using whole rock, 1040–1090 °C using melt inclusions, and >1100 °C using Rhyolite-MELTS, Figure 6a). Except for Matahi, that records deeper pressures (0.6–0.7 GPa), the magmas of these eruptions are mostly stored at 0.1–0.3 GPa, with evidence for magmas as deep as 0.6 GPa (Figure 6b). Given the large model uncertainties, individual magma reservoirs cannot be distinguished. However, despite the similar pre-eruptive compositions and conditions of Basalt-1, there is a wide variation in eruption style, and therefore no systematic relationship between storage conditions and eruption style (Figure 1b and Figure 6). Bamber et al. (2019) suggested moderate storage temperatures (<1100 °C) are important for generating basaltic Plinian eruptions, which occur at Tarawera, but are also found for the smaller intensity eruptions (Figure 6a).

Volatile concentrations (H_2O, Cl, and S) and trends are also similar between basaltic eruptions around the ŌVC (Figure 5). High H_2O concentrations suggest H_2O exsolution was important during ascent, which may drive basaltic Plinian eruptions (Bamber et al., 2019; Pérez et al., 2020). However, high H_2O concentrations are found across the range of eruption styles and are therefore not unique to Tarawera (Figure 5 and Figure 6c). Both Rotokawau and Tarawera have a population of melt inclusions that display degassing trends, and this population may have been missed at Terrace Rd where fewer melt inclusions were analysed. The unique degassing path for Plinian eruptions compared to other explosive eruptions proposed by Moretti et al. (2018) led to lower Cl but higher S in less explosive eruptions compared to more explosive eruptions due to the differences in dehydration and sulphide-saturation that occur during crystallisation. However, the observed differences in S_T and Cl concentration around the ŌVC do not relate to eruption style: Rotokawau has higher S_T and Cl but eruption intensity intermediate between Terrace Rd and Tarawera, and there is no evidence for sulphide-saturation (Figure 5). High CO_2 concentrations are thought to be important for generating (sub-)Plinian basaltic eruptions (e.g., Allison et al., 2021; Sable et al., 2009), which could be important around the ŌVC. Unfortunately, our CO_2 data for Tarawera are likely compromised by bubble formation and we do not have sufficient data to compare against smaller eruptions.

External influences within the crust could also influence eruption style of basaltic magmas around the ŌVC. Basaltic eruptions around the ŌVC are tectonically controlled, as evidenced by the linear nature of their eruptive vents underlain by dikes (Nairn and Cole, 1981). Hence, these eruptions may be triggered by earthquakes, especially given the high melt H_2O contents and mushy-nature of storage, which could also influence eruption style (e.g., Hamling and Kilgour, 2020; Seropian et al., 2021). Additionally, the presence and physical state (e.g., viscosity) of large silicic bodies in the crust could affect basaltic eruption style by impeding (or not) the ascent of basaltic magmas to the surface. The tectonics in addition to the complex nature of the crust around the ŌVC may therefore be important for generating the wide variety of basaltic eruption style observed in the region.

5.5 Mixing and entrainment during ascent influenced by eruption style

The occurrence of multiple compositional types of melts and crystals within single eruptions requires mixing and entrainment. This suggests that isolated pods of basaltic material evolve in the crust and are then assembled just prior to or during ascent and erupted at the surface (e.g., Cole et al., 2014; Leonard et al., 2002; Schmitz and Smith, 2004; Shane et al., 2008a, 2007). There is also evidence for sampling of previously erupted rhyolitic material during ascent. Textural evidence suggests variable extents of mixing between eruptions and short pre-eruptive timescales for mixing.

Firstly, there is evidence for the mixing of multiple basaltic magmas. Textures in the scoria are indicative of mixing between different batches of Basalt-1 and Basalt-2 that have subtly different crystallisation conditions (i.e., come from different places in the magmatic system) or decompression histories (e.g., T–H_2O conditions). At Tarawera, there are multiple instances of Basalt-1, including the carrier melt (as represented by the macrocryst-poor whole rock composition), and the low/high-S_T melt inclusions (Figure 5). A similar picture applies to Rotokawau, where mingled groundmass textures suggest multiple carrier melts from Basalt-1 (Figure 2c). For Terrace Rd, the small glomerocrysts could be phenocrystic or antecrystic, whereas the large glomerocrysts, as well as the large orthopyroxene crystals (Figure 2e, i, and m), are antecrystic. It is not clear whether all the antecrystic material came from the same place or event and how much melt was transported with the mixing event, although there is evidence for multiple melts in the groundmass. Additionally, all eruptions have antecrystic type one plagioclase from Basalt-2, with disequilibrium cores (coarse sieve textures) and a rim in equilibrium with the groundmass (Figure 2e–h). In all cases, the implication is that a carrier magma interacted with multiple different basaltic magma bodies as it ascended through the crust, picking up crystals *en route*. This is also seen in differences in oxygen isotope compositions between crystals and groundmass in these eruptions (Law et al., *in review*). The timescales of these interactions were likely very short (e.g., to preserve multiple groundmass textures and produce the sharp rims of type two plagioclase around type one plagioclase, Figure 2c and e–h), and probably occurred during pre-eruptive magma ascent.

The extent of mixing is correlated with eruption style. Lower intensity eruptions (Terrace Road, Rotokawau) contain a high proportion of macro-crystals, whereas Tarawera has a negligible crystal cargo (0.5 vol%, Sable et al., 2009). As crystals were entrained during ascent, the carrier melt entrained more crystals as it passed through the mushes prior to the smaller eruptions than to the Plinian eruption. This difference likely reflects the faster ascent rate of Plinian magmas, rather than the cause *per se* of varying eruption style.

All four studied eruptions additionally show entrainment of rhyolitic material (Figure 3 and Figure 4). The rhyolitic material appears to have been incorporated at a late-stage of magma ascent (e.g., sharp boundaries between basaltic and rhyolitic material, Figure 2p), probably when the basaltic magma punched through previously erupted, cold residual rhyolite domes (i.e., solid material). The other extreme is the Kaharoa eruption (and Rerewhakaaitu), where basaltic material is a minor component of a rhyolitic eruption (e.g., Leonard et al., 2002; Shane et al., 2007). This may highlight that slow ascent prevents basalts punching directly through rhyolite magma bodies, instead triggering rhyolitic eruption.

This diversity of magma types and mixing dynamics sampled both in individual eruptions and across eruptions from around the ŌVC reflects the interplay between basaltic magma ascent rates and the distribution, composition, and rheological state of magma bodies both vertically and horizontally. As mixing timescales appear to be short for the basalts that reach the surface, precursory signals to basaltic explosive eruptions could be limited, as suggested by the observations of the Tarawera 1886 C.E. eruption (Keam, 1988).

6 The magmatic architecture around the ŌVC

Combining the evidence from barometry and mixing textures suggests a crust full of individual magma reservoirs around the ŌVC, that are variously sampled during eruption. Despite large model uncertainties, pressures derived from clinopyroxene-melt and H_2O-CO_2 barometery and rhyolite-MELTS modelling lie within the TVZ crust assuming a crustal density of 2700 $kg{\cdot}m^{-3}$ and a Moho at 25–30 km or 0.7–0.8 GPa pressure (Bannister et al., 2004). This suggests that basaltic magmas, in addition to rhyolitic magmas, are stored and evolve polybarically within the crust. This agrees with current geochemical and geophysical constraints from previous

Tarawera clinopyroxene barometry (0.1–0.3 GPa, with some >0.7 GPa, reported in Sable et al., 2009) and the presence of partial melt bodies at similar depths around the ŌVC, such as at 6–16 km using receiver functions (Bannister et al., 2004), 10–20 km (as shallow as 8 km beneath Waimungu) using electrical resistivity inversions (Heise et al., 2016, 2010), and 8–10 km from earthquake swarms attributed to a basaltic dike intrusion (Benson et al., 2021). Additionally, conceptual models based on petrological modelling invoke mafic sheets residing at 11–15 km, with some isolated pods found at 8–6 km depths (Cole et al., 2014; Deering et al., 2010). Large uncertainties in clinopyroxene-melt barometry mean individual magma reservoirs cannot be identified using this method. However, the mineral textures and compositions suggest evolution in isolated reservoirs, where each batch has its own distinct composition reflecting their individual histories.

These observations suggest that a thick, crustal mush – containing a wealth of magma types in individual, isolated pockets – is mostly trapping the ascending basalts in the crust that fuel magmatism around the ŌVC. This model likely applies more generally to active calderas in the TVZ and is similar to other arc settings, such as the Andean Puna plateau, resulting in the dominance of compositionally-evolved volcanism (e.g., Delph et al., 2017; Kay et al., 2010). However, the extensional regime of the TVZ is clearly important in allowing some of these basalts to reach the surface and erupt explosively.

The few basalts that do make it to the surface have passed through the complicated crustal mush and carry the signature of these interactions in their crystal cargo. This highlights the use of basaltic mineral and melt inclusion chemistry as windows into the sub-surface in silicic magmatic regions, extending its application from using olivine-hosted melt inclusions to understand mantle melting dynamics (e.g., Barker et al., 2020) to analysing clinopyroxene-hosted melt inclusions to gain insight into crustal processes. Combining data from multiple eruptions separated spatially and temporally has highlighted that similar processes are important around the ŌVC for potentially the last ~30 ka.

7 Author Contributions

ECH, JDB, HMM, and GK conceived the project idea. ECH and SL collected and processed the data. All authors contributed to data interpretation. ECH led manuscript production with further contribution from all authors.

8 Acknowledgements

We would like to thank the Ruawahia 2B trust for welcoming us onto Mount Tarawera and permitting us to collect samples on the mountain and especially Ken Raureti, Tīpene Marr, and Paul Warbrick for their support of this work; Kaingaroa Timberlands for permits to access Kaingaroa Forest and Waimangu Forest to collect samples; Yves Feisel (now at the University of Mainz, Germany), Marco Michelini (now at the University of Pittsburgh, USA), Brad Scott (Te Pū Ao | GNS Science, Aotearoa New Zealand), Nick Macdonald (Te Pū Ao | GNS Science, Aotearoa New Zealand) for helping with basalt hunting; Richard Hinton for his assistance at the NERC ion microprobe facility at the University of Edinburgh, UK (IMF560/0515); Stuart Kearns and Ben Buse for their assistance with the electron probe and SEM at the University of Bristol, UK; two anonymous reviewers for their constructive review that improved the clarity and interpretation of the paper; and Prof. Mike Rowe (University of Auckland, Aotearoa New Zealand) for their editorial handling of the paper. ECH was supported by a NERC GW4+ DTP studentship (NE/L002434/1) and is thankful for the support and additional funding from CASE partner Te Pū Ao | GNS Science, Aotearoa New Zealand, and a Geology Option Post-Doctoral Fellowship from Caltech, CA USA. SL was supported by a NERC E^3 DTP studentship (NE/L002558/1). GK and ECH are supported by the Hazards and Risk Management Programme, which is part of New Zealand Strategic Science Investment Funding (SSIF) from the New Zealand Ministry of Business, Innovation & Employment (MBIE). JDB acknowledges support through a Royal Society Research Professorship.

9 References

Allan, A.S.R., Barker, S.J., Millet, M.A., Morgan, D.J., Rooyakkers, S.M., Schipper, C.I., Wilson, C.J.N., 2017. A cascade of magmatic events during the assembly and eruption of a super-sized magma body. Contrib. to Mineral. Petrol. 172, 49. https://doi.org/10.1007/s00410-017-1367-8

Allison, C.M., Roggensack, K., Clarke, A.B., 2021. Highly explosive basaltic eruptions driven by CO2 exsolution. Nat. Commun. 12, 217. https://doi.org/10.1038/s41467-020-20354-2

Annen, C., Blundy, J.D., Sparks, R.S.J., 2006. The Genesis of Intermediate and Silicic Magmas in Deep Crustal Hot Zones. J. Petrol. 47, 505–539. https://doi.org/10.1093/petrology/egi084

Bamber, E.C., Arzilli, F., Polacci, M., Hartley, M.E., Fellowes, J., Di Genova, D., Chavarría, D., Saballos, J.A., Burton, M.R., 2019. Pre- and syn-eruptive conditions of a basaltic Plinian eruption at Masaya Volcano, Nicaragua: The Masaya Triple Layer (2.1 ka). J. Volcanol. Geotherm. Res. 106761. https://doi.org/10.1016/J.JVOLGEORES.2019.106761

Bannister, S.C., Bryan, C.J., Bibby, H.M., 2004. Shear wave velocity variation across the Taupo Volcanic Zone, New Zealand, from receiver function inversion. Geophys. J. Int. 159, 291–310. https://doi.org/10.1111/j.1365-246X.2004.02384.x

Barker, S.J., Rowe, M.C., Wilson, C.J.N., Gamble, J.A., Rooyakkers, S.M., Wysoczanski, R.J., Illsley-Kemp, F., Kenworthy, C.C., 2020. What lies beneath? Reconstructing the primitive magmas fueling voluminous silicic volcanism using olivine-hosted melt inclusions. Geology 48, 504–508. https://doi.org/10.1130/G47422.1

Barth, A., Newcombe, M., Plank, T., Gonnermann, H., Hajimirza, S., Soto, G.J., Saballos, A., Hauri, E., 2019. Magma decompression rate correlates with explosivity at basaltic volcanoes — Constraints from water diffusion in olivine. J. Volcanol. Geotherm. Res. 387, 106664. https://doi.org/10.1016/j.jvolgeores.2019.106664

Barth, A., Plank, T., 2021. The Ins and Outs of Water in Olivine-Hosted Melt Inclusions: Hygrometer vs. Speedometer. Front. Earth Sci. 9, 343. https://doi.org/10.3389/feart.2021.614004

Beanland, S., 1989. The Rotokawau Basalt. University of Otago.

Beanland, S., Houghton, B.F., 1978. Rotokawau Tephra : basaltic maars in Okataina Volcanic Centre, Taupo volcanic zone. New Zeal. Geol. Surv. Bull. 37–43.

Benson, T.W., Illsley-Kemp, F., Elms, H.C., Hamling, I.J., Savage, M.K., Wilson, C.J.N., Mestel, E.R.H., Barker, S.J., 2021. Earthquake Analysis Suggests Dyke Intrusion in 2019 Near Tarawera Volcano, New Zealand. Front. Earth Sci. 8, 604. https://doi.org/10.3389/feart.2020.606992

Blatter, D.L., Sisson, T.W., Hankins, W. Ben, 2013. Crystallization of oxidized, moderately hydrous arc basalt at mid- to lower-crustal pressures: implications for andesite genesis. Contrib. to Mineral. Petrol. 166, 861–886. https://doi.org/10.1007/s00410-013-0920-3

Bowyer, D.A., 2001. Petrologic, Geochemical and Isotopic Evolution of Rhyolite Lavas from the Okataina, Rotorua and Kapenga Volcanic Centres, Taupo Volcanic Zone, New Zealand. University of Waikato.

Bucholz, C.E., Gaetani, G.A., Behn, M.D., Shimizu, N., 2013. Post-entrapment modification of volatiles and oxygen fugacity in olivine-hosted melt inclusions. Earth Planet. Sci. Lett. 374, 145–155. https://doi.org/10.1016/j.epsl.2013.05.033

Buck, C.E., Higham, T.F.G., Lowe, D.J., 2003. Bayesian tools for tephrochronology: http://dx.doi.org/10.1191/0959683603hl652ft 13, 639–647. https://doi.org/10.1191/0959683603HL652FT

Burt, R.M., Brown, S.J.A., Cole, J.W., Shelley, D., Waight, T.E., 1998. Glass-bearing plutonic fragments from ignimbrites of the Okataina caldera complex, Taupo Volcanic Zone, New Zealand: remnants of a partially molten intrusion associated with preceding eruptions. J. Volcanol. Geotherm. Res. 84, 209–237. https://doi.org/10.1016/S0377-0273(98)00039-0

Carey, R.J., Houghton, B.F., Sable, J.E., Wilson, C.J.N., 2007. Contrasting grain size and componentry in complex proximal deposits of the 1886 Tarawera basaltic Plinian eruption. Bull. Volcanol. 69, 903–926. https://doi.org/10.1007/s00445-007-0117-6

Clemente, B., SCAILLET, B., PICHAVANT, M., 2004. The Solubility of Sulphur in Hydrous Rhyolitic Melts. J. Petrol. 45, 2171–2196. https://doi.org/10.1093/petrology/egh052

Cole, J.W., 1979. Structure, petrology, and genesis of Cenozoic volcanism, Taupo Volcanic Zone, New Zealand—a review. New Zeal. J. Geol. Geophys. 22, 631–657. https://doi.org/10.1080/00288306.1979.10424173

Cole, J.W., 1973a. High-alumina basalts of Taupo Volcanic Zone, New Zealand. Lithos 6, 53–64. https://doi.org/10.1016/0024-4937(73)90079-0

Cole, J.W., 1973b. High-alumina basalts of Taupo Volcanic Zone, New Zealand. LITHOS 6, 53–64. https://doi.org/10.1016/0024-4937(73)90079-0

Cole, J.W., 1970a. Structure and eruptive history of the Tarawera Volcanic Complex. New Zeal. J. Geol. Geophys. 13, 879–902. https://doi.org/10.1080/00288306.1970.10418208

Cole, J.W., 1970b. Petrology of the basic rocks of the Tarawera Volcanic Complex. New Zeal. J. Geol. Geophys. 13, 925–936. https://doi.org/10.1080/00288306.1970.10418210

Cole, J.W., Deering, C.D., Burt, R.M., Sewell, S., Shane, P.A., Matthews, N.E., 2014. Okataina Volcanic Centre, Taupo Volcanic Zone, New Zealand: A review of volcanism and synchronous pluton development in an active, dominantly silicic caldera system. Earth-Science Rev. 128, 1–17. https://doi.org/10.1016/j.earscirev.2013.10.008

Danyushevsky, L., Della-Pasqua, F.N., Sokolov, S., 2000. Re-equilibration of melt inclusions trapped by magnesian olivine phenocrysts from subduction-related magmas: Petrological implications. Contrib. to Mineral. Petrol. 138, 68–83. https://doi.org/10.1007/PL00007664

Danyushevsky, L., Sobolev, A.V., Dmitriev, L.V., 1988. Orthopyroxene-bearing low-Ti tholeiites: The new type of ceanic ridge tholeiite. Trans. USSR Acad. Sci. Earth Sci. Sect. 292, 102–105.

Darragh, M.B., Cole, J.W., Nairn, I.A., Shane, P.A., 2006. Pyroclastic stratigraphy and eruption dynamics of the 21.9 ka Okareka and 17.6 ka Rerewhakaaitu eruption episodes from Tarawera Volcano, Okataina Volcanic Centre, New Zealand. New Zeal. J. Geol. Geophys. 49, 309–328. https://doi.org/10.1080/00288306.2006.9515170

Davis, W.J., 1985. Geochemistry and petrology of the Rotoiti and Earthquake Flat pyroclastic deposits. University of Auckland.

Deering, C.D., Cole, J.W., Vogel, T.A., 2011. Extraction of crystal-poor rhyolite from a hornblende-bearing intermediate mush: A case study of the caldera-forming Matahina eruption, Okataina volcanic complex. Contrib. to Mineral. Petrol. 161, 129–151. https://doi.org/10.1007/s00410-010-0524-0

Deering, C.D., Gravley, D.M., Vogel, T.A., Cole, J.W., Leonard, G.S., 2010. Origins of cold-wet-oxidizing to hot-dry-reducing rhyolite magma cycles and distribution in the Taupo Volcanic Zone, New Zealand. Contrib. to Mineral. Petrol. 160, 609–629. https://doi.org/10.1007/s00410-010-0496-0

Delph, J.R., Ward, K.M., Zandt, G., Ducea, M.N., Beck, S.L., 2017. Imaging a magma plumbing system from MASH zone to magma reservoir. Earth Planet. Sci. Lett. 457, 313–324. https://doi.org/10.1016/J.EPSL.2016.10.008

Ducea, M.N., Saleeby, J.B., Bergantz, G., 2015. The Architecture, Chemistry, and Evolution of Continental Magmatic Arcs. http://dx.doi.org/10.1146/annurev-earth-060614-105049 43, 299–331. https://doi.org/10.1146/ANNUREV-EARTH-060614-105049

Dungan, M.A., Rhodes, J.M., 1978. Residual glasses and melt inclusions in basalts from DSDP Legs 45 and 46: Evidence for magma mixing. Contrib. to Mineral. Petrol. 67, 417–431. https://doi.org/10.1007/BF00383301

Foden, J.D., Green, D.H., 1992. Possible role of amphibole in the origin of andesite: some experimental and natural evidence. Contrib. to Mineral. Petrol. 109, 479–493. https://doi.org/10.1007/BF00306551

Froggatt, P.C., Lowe, D.J., 1990. A review of late Quaternary silicic and some other tephra formations from New Zealand: Their stratigraphy, nomenclature, distribution, volume, and age. New Zeal. J. Geol. Geophys. 33, 89–109. https://doi.org/10.1080/00288306.1990.10427576

Gaetani, G.A., O'Leary, J.A., Shimizu, N., Bucholz, C.E., Newville, M., 2012. Rapid reequilibration of H2O and oxygen fugacity in olivine-hosted melt inclusions. Geology 40, 915–918. https://doi.org/10.1130/G32992.1

Gaetani, G.A., Watson, E.B., 2002. Modeling the major-element evolution of olivine-hosted melt inclusions. Chem. Geol. 183, 25–41. https://doi.org/10.1016/S0009-2541(01)00370-9

Gaetani, G.A., Watson, E.B., 2000. Open system behavior of olivine-hosted melt inclusions. Earth Planet. Sci. Lett. 183, 27–41. https://doi.org/10.1016/S0012-821X(00)00260-0

Gamble, J.A., Smith, I.E.M., Graham, I.J., Peter Kokelaar, B., Cole, J.W., Houghton, B.F., Wilson, C.J.N., 1990. The petrology, phase relations and tectonic setting of basalts from the taupo volcanic zone, New Zealand and the Kermadec Island arc - havre trough, SW Pacific. J. Volcanol. Geotherm. Res. 43, 253–270. https://doi.org/10.1016/0377-0273(90)90055-K

Gamble, J.A., Smith, I.E.M., McCulloch, M.T., Graham, I.J., Kokelaar, B.P., 1993. The geochemistry and petrogenesis of basalts from the Taupo Volcanic Zone and Kermadec Island Arc, S.W. Pacific. J. Volcanol. Geotherm. Res. 54, 265–290. https://doi.org/10.1016/0377-0273(93)90067-2

Gennaro, E., Paonita, A., Iacono-Marziano, G., Moussallam, Y., Pichavant, M., Peters, N., Martel, C., 2021. Sulphur Behaviour and Redox Conditions in Etnean Magmas during Magma Differentiation and Degassing. J. Petrol. 61. https://doi.org/10.1093/PETROLOGY/EGAA095

Ghiorso, M.S., Gualda, G.A.R., 2015. An H_2O–CO_2 mixed fluid saturation model compatible with rhyolite-MELTS. Contrib. to Mineral. Petrol. 169, 53. https://doi.org/10.1007/s00410-015-1141-8

Graham, I.J., Cole, J.W., Briggs, R.M., Gamble, J.A., Smith, I.E.M., 1995. Petrology and petrogenesis of volcanic rocks from the Taupo Volcanic Zone: a review. J. Volcanol. Geotherm. Res. 68, 59–87. https://doi.org/10.1016/0377-0273(95)00008-I

Grange, L.I., 1937. The geology of the Rotorua-Taupo Subdivision, Rotorua and Kaimanawa Divisions. New Zeal. Geol. Surv. Bull. 37, 1–138.

Grove, T.L., Till, C.B., Krawczynski, M.J., 2012. The Role of H_2O in Subduction Zone Magmatism. http://dx.doi.org/10.1146/annurev-earth-042711-105310 40, 413–439. https://doi.org/10.1146/ANNUREV-EARTH-042711-105310

Gualda, G.A.R., Ghiorso, M.S., Lemons, R. V., Carley, T.L., 2012. Rhyolite-MELTS: a Modified Calibration of MELTS Optimized for Silica-rich, Fluid-bearing Magmatic Systems. J. Petrol. 53, 875–890. https://doi.org/10.1093/PETROLOGY/EGR080

Hamada, M., Fujii, T., 2007. H_2O-rich island arc low-K tholeiite magma inferred from Ca-rich plagioclase-melt inclusion equilibria. Geochemical Journal2 41, 437–461.

Hamling, I.J., Kilgour, G., 2020. Goldilocks conditions required for earthquakes to trigger basaltic eruptions: Evidence from the 2015 Ambrym eruption. Sci. Adv. 6, eaaz5261. https://doi.org/10.1126/SCIADV.AAZ5261

Hartley, M.E., Maclennan, J., Edmonds, M., Thordarson, T., 2014. Reconstructing the deep CO_2 degassing behaviour of large basaltic fissure eruptions. Earth Planet. Sci. Lett. 393, 120–131. https://doi.org/10.1016/j.epsl.2014.02.031

Hartley, M.E., Neave, D.A., Maclennan, J., Edmonds, M., Thordarson, T., 2015. Diffusive over-hydration of olivine-hosted melt inclusions. Earth Planet. Sci. Lett. 425, 168–178. https://doi.org/10.1016/J.EPSL.2015.06.008

Heise, W., Caldwell, T.G., Bertrand, E.A., Hill, G.J., Bennie, S.L., Palmer, N.G., 2016. Imaging the deep source of the Rotorua and Waimangu geothermal fields, Taupo Volcanic Zone, New Zealand. J. Volcanol. Geotherm. Res. 314, 39–48. https://doi.org/10.1016/j.jvolgeores.2015.10.017

Heise, W., Caldwell, T.G., Bibby, H.M., Bennie, S.L., 2010. Three-dimensional electrical resistivity image of magma beneath an active continental rift, Taupo Volcanic Zone, New Zealand. Geophys. Res. Lett. 37, n/a-n/a. https://doi.org/10.1029/2010GL043110

Hiess, J., Cole, J.W., Spinks, K.D., 2007. Influence of the crust and crustal structure on the location and composition of high-alumina basalts of the Taupo Volcanic Zone, New Zealand. New Zeal. J. Geol. Geophys. 50, 327–342. https://doi.org/10.1080/00288300709509840

Hogg, A.G., Higham, T.F.G., Lowe, D.J., Palmer, J.G., Reimer, P.J., Newnham, R.M., 2003. A wiggle-match date for Polynesian settlement of New Zealand. Antiquity 77, 116–125. https://doi.org/10.1017/S0003598X00061408

Hopkins, J.L., Lowe, D.J., Horrocks, J.L., 2021. Tephrochronology in Aotearoa New Zealand. https://doi.org/10.1080/00288306.2021.1908368 64, 153–200. https://doi.org/10.1080/00288306.2021.1908368

Houghton, B.F., Hackett, W.R., 1984. Strombolian and phreatomagmatic deposits of Ohakune craters, Ruapehu, New Zealand: A complex interaction between external water and rising basaltic magma. J. Volcanol. Geotherm. Res. 21, 207–231. https://doi.org/10.1016/0377-0273(84)90023-4

Houghton, B.F., Wilson, C.J.N., 1989. A vesicularity index for pyroclastic deposits. Bull. Volcanol. 51, 451–462. https://doi.org/10.1007/BF01078811

Houghton, B.F., Wilson, C.J.N., McWilliams, M.O., Lanphere, M.A., Weaver, S.D., Briggs, R.M., Pringle, M.S., 1995. Chronology and dynamics of a large silicic magmatic system: central Taupo Volcanic Zone, New Zealand. Geology 23, 13–16. https://doi.org/10.1130/0091-7613(1995)023<0013:CADOAL>2.3.CO;2

Hughes, E.C., Buse, B., Kearns, S.L., Blundy, J.D., Kilgour, G., Mader, H.M., 2019a. Low analytical totals in EPMA of hydrous silicate glass due to sub-surface charging: Obtaining accurate volatiles by difference. Chem. Geol. 505, 48–56. https://doi.org/10.1016/J.CHEMGEO.2018.11.015

Hughes, E.C., Mazot, A., Kilgour, G., Asher, C., Michelini, M., Britten, K., Chardot, L., Feisel, Y., Werner, C., 2019b. Understanding Degassing Pathways Along the 1886 Tarawera (New Zealand) Volcanic Fissure by Combining Soil and Lake CO_2 Fluxes. Front. Earth Sci. 7, 264. https://doi.org/10.3389/feart.2019.00264

Iacovino, K., Till, C., 2018. DensityX: A program for calculating the densities of hydrous magmatic liquids from 427-1,627 °C and up to 30 kbar. Volcanica 2, 1–10. https://doi.org/10.30909/vol.02.01.0110

Jackson, M.D., Blundy, J., Sparks, R.S.J., 2018. Chemical differentiation, cold storage and remobilization of magma in the Earth's crust. Nature 564, 405–409. https://doi.org/10.1038/s41586-018-0746-2

Johnson, E.R., Kamenetsky, V.S., McPhie, J., Wallace, P.J., 2011. Degassing of the H_2O-rich rhyolites of the Okataina Volcanic Center, Taupo Volcanic Zone, New Zealand. Geology 39, 311–314. https://doi.org/10.1130/G31543.1

Kay, S.M., Coira, B.L., Caffe, P.J., Chen, C.H., 2010. Regional chemical diversity, crustal and mantle sources and evolution of central Andean Puna plateau ignimbrites. J. Volcanol. Geotherm. Res. 198, 81–111. https://doi.org/10.1016/J.JVOLGEORES.2010.08.013

Keam, R.F., 1988. Tarawera: The volcanic eruption of 10 June 1886 A.D. Published by the author, Auckland.

Kress, V.C., Carmichael, I.S.E., 1991. The compressibility of silicate liquids containing Fe_2O_3 and the effect of composition, temperature, oxygen fugacity and pressure on their redox states. Contrib. to Mineral. Petrol. 108, 82–92. https://doi.org/10.1007/BF00307328

Laumonier, M., Scaillet, B., Pichavant, M., Champallier, R., Andujar, J., Arbaret, L., 2014. On the conditions of magma mixing and its bearing on andesite production in the crust. Nat. Commun. 2014 51 5, 1–12. https://doi.org/10.1038/ncomms6607

Law, S., Bromiley, G.D., Kilgour, G.N., Fitton, J.G., 2021. Tracing mantle source variation through xenocrystic olivine in the Taupo Volcanic Zone, New Zealand: A role for lithospheric mantle in the shift from andesitic to rhyolitic compositions. Lithos 394–395, 106185. https://doi.org/10.1016/J.LITHOS.2021.106185

Law, S., Kilgour, G., Bromiley, G.D., Boyce, A.J., n.d. Along arc variation in monogenetic mafic magmas from the Taupo Volcanic Zone, New Zealand: Insights from the crystal cargo and oxygen isotopes. J. Petrol.

Leonard, G.S., Cole, J.W., Nairn, I.A., Self, S., 2002. Basalt triggering of the c. AD 1305 Kaharoa rhyolite eruption, Tarawera Volcanic Complex, New Zealand. J. Volcanol. Geotherm. Res. 115, 461–486. https://doi.org/10.1016/S0377-0273(01)00326-2

Lloyd, A.S., Plank, T., Ruprecht, P., Hauri, E.H., Rose, W., 2013. Volatile loss from melt inclusions in pyroclasts of differing sizes. Contrib. to Mineral. Petrol. 165, 129–153. https://doi.org/10.1007/s00410-012-0800-2

Lowenstern, J.B., 2003. Melt inclusions come of age: Volatiles, volcanoes, and Sorby's legacy. Dev. Volcanol. 5, 1–21. https://doi.org/10.1016/S1871-644X(03)80021-9

Lowenstern, J.B., 1995. Applications of silicate-melt inclusions to the study of magmatic volatiles, in: Thompson, J.F.. (Ed.), Magmas, Fluids and Ore Deposits. Mineralogical Assoication of Canada Short Course Volume No.23. pp. 71–99.

Maclennan, J., 2017. Bubble formation and decrepitation control the CO_2 content of olivine-hosted melt inclusions. Geochemistry, Geophys. Geosystems 18, 597–616. https://doi.org/10.1002/2016GC006633

Mangan, M.T., Sisson, T.W., Hankins, W. Ben, Shimizu, N., Vennemann, T., 2021. Constraints on deep, CO_2-rich degassing at arc volcanoes from solubility experiments on hydrous basaltic andesite of Pavlof Volcano, Alaska Peninsula, at 300 to 1200 MPa. Am. Mineral. 106, 762–773. https://doi.org/10.2138/am-2021-7531

Marxer, F., Ulmer, · Peter, Müntener, · Othmar, 2021. Polybaric fractional crystallisation of arc magmas: an experimental study simulating trans-crustal magmatic systems. Contrib. to Mineral. Petrol. 2021 1771 177, 1–36. https://doi.org/10.1007/S00410-021-01856-8

Mazot, A., Schwandner, F.M., Christenson, B., de Ronde, C.E.J., Inguaggiato, S., Scott, B.J., Graham, D., Britten, K., Keeman, J., Tan, K., 2014. CO_2 discharge from the bottom of volcanic Lake Rotomahana, New Zealand. Geochemistry, Geophys. Geosystems 15, 577–588. https://doi.org/10.1002/2013GC004945

Moore, L.R., Gazel, E., Tuohy, R., Lloyd, A.S., Esposito, R., Steele-MacInnis, M., Hauri, E.H., Wallace, P.J., Plank, T., Bodnar, R.J., 2015. Bubbles matter: An assessment of the contribution of vapor bubbles to melt inclusion volatile budgets. Am. Mineral. 100, 806–823. https://doi.org/10.2138/am-2015-5036

Moretti, R., Métrich, N., Arienzo, I., Di Renzo, V., Aiuppa, A., Allard, P., 2018. Degassing vs. eruptive styles at Mt. Etna volcano (Sicily, Italy). Part I: Volatile stocking, gas fluxing, and the shift from low-energy to highly explosive basaltic eruptions. Chem. Geol. 482, 1–17. https://doi.org/10.1016/J.CHEMGEO.2017.09.017

Mortimer, N., Campbell, H.J., Tulloch, A.J., King, P.R., Stagpoole, V.M., Wood, R.A., Rattenbury, M.S., Sutherland, R., Adams, C.J., Collot, J., Seton, M., 2017. Zealandia: Earth's hidden Continent. GSA Today 27, 27–35. https://doi.org/10.1130/GSATG321A.1

Müntener, O., Ulmer, P., 2018a. Arc crust formation and differentiation constrained by experimental petrology. Am. J. Sci. 318, 64–89. https://doi.org/10.2475/01.2018.04

Müntener, O., Ulmer, P., 2018b. Arc crust formation and differentiation constrained by experimental petrology. Am. J. Sci. 318, 64–89. https://doi.org/10.2475/01.2018.04

Nairn, I.A., 2002. Geology of the Okataina Volcanic Centre, scale 1:50 000. Institute of Geological and Nuclear Sciences Limited.

Nairn, I.A., 1992. The Te Rere and Okareka eruptive episodes — Okataina Volcanic Centre, Taupo Volcanic

Zone, New Zealand. New Zeal. J. Geol. Geophys. 35, 93–108. https://doi.org/10.1080/00288306.1992.9514503

Nairn, I.A., 1981. Some Studies of the Geology, Volcanic History, and Geothermal Resources of the Okataina Volcanic Centre, Taupo Volcanic Zone, New Zealand. Victoria University of Wellington, Wellington.

Nairn, I.A., 1979. Rotomahana—Waimangu eruption, 1886: base surge and basalt magma. New Zeal. J. Geol. Geophys. 22, 363–378. https://doi.org/10.1080/00288306.1979.10424105

Nairn, I.A., Cole, J.W., 1981. Basalt dikes in the 1886 Tarawera Rift. New Zeal. J. Geol. Geophys. 24, 585–592. https://doi.org/10.1080/00288306.1981.10421534

Nairn, I.A., Self, S., Cole, J.W., Leonard, G.S., Scutter, C., 2001. Distribution, stratigraphy, and history of proximal deposits from the c. AD 1305 Kaharoa eruptive episode at Tarawera Volcano, New Zealand. New Zeal. J. Geol. Geophys. 44, 467–484. https://doi.org/10.1080/00288306.2001.9514950

Nairn, I.A., Shane, P.A., Cole, J.W., Leonard, G.., Self, S., Pearson, N., 2004. Rhyolite magma processes of the ~AD 1315 Kaharoa eruption episode, Tarawera volcano, New Zealand. J. Volcanol. Geotherm. Res. 131, 265–294. https://doi.org/10.1016/S0377-0273(03)00381-0

Nandedkar, R.H., Ulmer, P., Müntener, O., 2014. Fractional crystallization of primitive, hydrous arc magmas: An experimental study at 0.7 GPa. Contrib. to Mineral. Petrol. 167, 1–27. https://doi.org/10.1007/s00410-014-1015-5

Neave, D.A., Putirka, K.D., 2017. A new clinopyroxene-liquid barometer, and implications for magma storage pressures under Icelandic rift zones. Am. Mineral. 102, 777–794. https://doi.org/10.2138/am-2017-5968

Newnham, R.M., Eden, D.N., Lowe, D.J., Hendy, C.H., 2003. Rerewhakaaitu Tephra, a land–sea marker for the Last Termination in New Zealand, with implications for global climate change. Quat. Sci. Rev. 22, 289–308. https://doi.org/10.1016/S0277-3791(02)00137-3

Nielsen, R.L., Michael, P.J., Sours-Page, R., 1998. Chemical and physical indicators of compromised melt inclusions. Geochim. Cosmochim. Acta 62, 831–839. https://doi.org/10.1016/S0016-7037(98)00024-6

O'Neill, H., 2020. The thermodynamic controls on sulfide saturation in silicate melts with application to Ocean Floor Basalts. https://doi.org/10.1002/ESSOAR.10503096.1

Panjasawatwong, Y., Danyushevsky, L. V., Crawford, A.J., Harris, K.L., 1995. An experimental study of the effects of melt composition on plagioclase-melt equilibria at 5 and 10 kbar: implications for the origin of magmatic high-An plagioclase. Contrib. to Mineral. Petrol. 118, 420–432. https://doi.org/10.1007/s004100050024

Pérez, W., Freundt, A., Kutterolf, S., 2020. The basaltic plinian eruption of the ~6 ka San Antonio Tephra and formation of the Masaya caldera, Nicaragua. J. Volcanol. Geotherm. Res. 401, 106975. https://doi.org/10.1016/j.jvolgeores.2020.106975

Peti, L., Hopkins, J.L., Augustinus, P.C., 2021. Revised tephrochronology for key tephras in the 130-ka Ōrākei Basin maar core, Auckland Volcanic Field, New Zealand: implications for the timing of climatic changes. https://doi.org/10.1080/00288306.2020.1867200 64, 235–249. https://doi.org/10.1080/00288306.2020.1867200

Pittari, A., Muir, S.L., Hendy, C.H., 2016. Lake-floor sediment texture and composition of a hydrothermally-active, volcanic lake, Lake Rotomahana. J. Volcanol. Geotherm. Res. 314, 169–181. https://doi.org/10.1016/j.jvolgeores.2016.02.025

Price, R.C., Gamble, J.A., Smith, I.E.M., Stewart, R.B., Eggins, S., Wright, I.C., 2005. An integrated model for the temporal evolution of andesites and rhyolites and crustal development in New Zealand's North Island. J. Volcanol. Geotherm. Res. 140, 1–24. https://doi.org/10.1016/j.jvolgeores.2004.07.013

Pullar, W.A., Nairn, I.A., 1972. Matahi Basaltic Tephra member, Rotoiti Breccia Formation. New Zeal. J. Geol. Geophys. 15, 446–450. https://doi.org/10.1080/00288306.1972.10422342

Putirka, K.D., 2008. Thermometers and Barometers for Volcanic Systems. Rev. Mineral. Geochemistry 69, 61–120. https://doi.org/10.2138/rmg.2008.69.3

Rasmussen, D.J., Plank, T.A., Wallace, P.J., Newcombe, M.E., Lowenstern, J.B., 2020. Vapor-bubble growth in olivine-hosted melt inclusions. Am. Mineral. 105, 1898–1919. https://doi.org/10.2138/am-2020-7377

Roedder, E., 1979. Origin and significance of magmatic inclusions. Bull. Mineral. 102, 487–510.

Rooney, T.O., Deering, C.D., 2014. Conditions of melt generation beneath the Taupo Volcanic Zone: The influence of heterogeneous mantle inputs on large-volume silicic systems. Geology 42, 3–6. https://doi.org/10.1130/G34868.1

Rooyakkers, S.M., Wilson, C.J.N., Schipper, C.I., Barker, S.J., Allan, A.S.R., 2018. Textural and micro-analytical insights into mafic–felsic interactions during the Oruanui eruption, Taupo. Contrib. to Mineral. Petrol. 173, 35. https://doi.org/10.1007/s00410-018-1461-6

Rose-Koga, E.F., Bouvier, A.S., Gaetani, G.A., Wallace, P.J., Allison, C.M., Andrys, J.A., Angeles de la Torre, C.A., Barth, A., Bodnar, R.J., Bracco Gartner, A.J.J., Butters, D., Castillejo, A., Chilson-Parks, B., Choudhary, B.R., Cluzel, N., Cole, M., Cottrell, E., Daly, A., Danyushevsky, L. V., DeVitre, C.L., Drignon, M.J., France, L., Gaborieau, M., Garcia, M.O., Gatti, E., Genske, F.S., Hartley, M.E., Hughes, E.C., Iveson, A.A., Johnson, E.R., Jones, M., Kagoshima, T., Katzir, Y., Kawaguchi, M., Kawamoto, T., Kelley, K.A., Koornneef, J.M., Kurz, M.D., Laubier, M., Layne, G.D., Lerner, A., Lin, K.Y., Liu, P.P., Lorenzo-Merino, A., Luciani, N., Magalhães, N., Marschall, H.R., Michael, P.J., Monteleone, B.D., Moore, L.R., Moussallam, Y., Muth, M., Myers, M.L., Narváez, D.F., Navon, O., Newcombe, M.E., Nichols, A.R.L., Nielsen, R.L., Pamukcu, A., Plank, T., Rasmussen, D.J., Roberge, J., Schiavi, F., Schwartz, D., Shimizu, K., Shimizu, N., Thomas, J.B., Thompson, G.T., Tucker, J.M., Ustunisik, G., Waelkens, C., Zhang, Y., Zhou, T., 2021. Silicate melt inclusions in the new millennium: A review of recommended practices for preparation, analysis, and data presentation. Chem. Geol. 570, 120145. https://doi.org/10.1016/j.chemgeo.2021.120145

Rowe, M.C., Carey, R.J., White, J.D.L., Kilgour, G., Hughes, E., Ellis, B., Rosseel, J.-B., Segovia, A., 2021. Tarawera 1886: an integrated review of volcanological and geochemical characteristics of a complex basaltic eruption. New Zeal. J. Geol. Geophys. 64, 296–319. https://doi.org/10.1080/00288306.2021.1914118

Sable, J.E., Houghton, B.F., Wilson, C.J.N., Carey, R.J., 2009. Eruption Mechanisms during the climax of the Tarawera 1886 basaltic Plinian eruption inferred from microtextural characteristics of the deposits, in: Thordarson, T., Self, S., Larsen, G., Rowland, S.K., Hoskuldsson, A. (Eds.), Studies in Volcanology: The Legacy of John Walker. The Geological Society of London, London, pp. 129–154.

Saper, L.M., Stolper, E.M., 2020. Controlled Cooling-Rate Experiments on Olivine-Hosted Melt Inclusions: Chemical Diffusion and Quantification of Eruptive Cooling Rates on Hawaii and Mars. Geochemistry, Geophys. Geosystems 21. https://doi.org/10.1029/2019GC008772

Sas, M., Shane, P., Kuritani, T., Zellmer, G.F., Kent, A.J.R., Nakagawa, M., 2021. Mush, melts and metasediments: A history of rhyolites from the Okataina Volcanic Centre, New Zealand, as captured in plagioclase. J. Petrol. https://doi.org/10.1093/petrology/egab038

Schiano, P., 2003. Primitive mantle magmas recorded as silicate melt inclusions in igneous minerals. Earth-Science Rev. 63, 121–144. https://doi.org/10.1016/S0012-8252(03)00034-5

Schmitz, M.D., Smith, I.E.M., 2004. The Petrology of the Rotoiti Eruption Sequence, Taupo Volcanic Zone: an Example of Fractionation and Mixing in a Rhyolitic System. J. Petrol. 45, 2045–2066. https://doi.org/10.1093/petrology/egh047

Seropian, G., Kennedy, B.M., Walter, T.R., Ichihara, M., Jolly, A.D., 2021. A review framework of how earthquakes trigger volcanic eruptions. Nat. Commun. 12, 1–13. https://doi.org/10.1038/s41467-021-21166-8

Shane, P.A., Martin, S.B., Smith, V.C., Beggs, K.F., Darragh, M.B., Cole, J.W., Nairn, I.A., 2007. Multiple rhyolite magmas and basalt injection in the 17.7 ka Rerewhakaaitu eruption episode from Tarawera volcanic complex, New Zealand. J. Volcanol. Geotherm. Res. 164, 1–26. https://doi.org/10.1016/j.jvolgeores.2007.04.003

Shane, P.A., Nairn, I.A., Smith, V.C., 2005. Magma mingling in the ∼50 ka Rotoiti eruption from Okataina Volcanic Centre: implications for geochemical diversity and chronology of large volume rhyolites. J. Volcanol. Geotherm. Res. 139, 295–313. https://doi.org/10.1016/j.jvolgeores.2004.08.012

Shane, P.A., Nairn, I.A., Smith, V.C., Darragh, M.B., Beggs, K.F., Cole, J.W., 2008a. Silicic recharge of multiple rhyolite magmas by basaltic intrusion during the 22.6 ka Okareka Eruption Episode, New Zealand. Lithos 103, 527–549. https://doi.org/10.1016/j.lithos.2007.11.002

Shane, P.A., Smith, V.C., Nairn, I.A., 2008b. Millennial timescale resolution of rhyolite magma recharge at Tarawera volcano: insights from quartz chemistry and melt inclusions. Contrib. to Mineral. Petrol. 156, 397–411. https://doi.org/10.1007/s00410-008-0292-2

Smith, V.C., Shane, P., Nairn, I.A., 2004. Reactivation of a rhyolitic magma body by new rhyolitic intrusion before the 15.8 ka Rotorua eruptive episode: implications for magma storage in the Okataina Volcanic Centre, New Zealand. J. Geol. Soc. London. 161, 757–772. https://doi.org/10.1144/0016-764903-092

Smith, V.C., Shane, P.A., Nairn, I.A., 2005. Trends in rhyolite geochemistry, mineralogy, and magma storage during the last 50 kyr at Okataina and Taupo volcanic centres, Taupo Volcanic Zone, New Zealand. J. Volcanol. Geotherm. Res. 148, 372–406. https://doi.org/10.1016/j.jvolgeores.2005.05.005

Sobolev, A. V., Shimizu, N., 1993. Ultra-depleted primary melt included in an olivine from the Mid-Atlantic Ridge. Nature 363, 151–154. https://doi.org/10.1038/363151a0

Sparks, S.R.J., Sigurdsson, H., Wilson, L., 1977. Magma mixing: a mechanism for triggering acid explosive eruptions. Nat. 1977 2675609 267, 315–318. https://doi.org/10.1038/267315a0

Storm, S., Shane, P., Schmitt, A.K., Lindsay, J.M., 2011. Contrasting punctuated zircon growth in two syn-erupted rhyolite magmas from Tarawera volcano: Insights to crystal diversity in magmatic systems. Earth Planet. Sci. Lett. 301, 511–520. https://doi.org/10.1016/J.EPSL.2010.11.034

Takagi, D., Sato, H., Nakagawa, M., 2005. Experimental study of a low-alkali tholeiite at 1-5 kbar: Optimal condition for the crystallization of high-An plagioclase in hydrous arc tholeiite. Contrib. to Mineral. Petrol. 149, 527–540. https://doi.org/10.1007/s00410-005-0666-7

Tattitch, B., Chelle-Michou, C., Blundy, J., Loucks, R.R., 2021. Chemical feedbacks during magma degassing control chlorine partitioning and metal extraction in volcanic arcs. Nat. Commun. 2021 121 12, 1–11. https://doi.org/10.1038/s41467-021-21887-w

Thomas, A.P.W., 1888. Report on the Eruption of Tarawera and Rotomahana, NZ, Government Printer, Wellington, New Zealand.

Thomas, R.W., Wood, B.J., 2021. The chemical behaviour of chlorine in silicate melts. Geochim. Cosmochim. Acta 294, 28–42. https://doi.org/10.1016/J.GCA.2020.11.018

Waight, T.E., Troll, V.R., Gamble, J.A., Price, R.C., Chadwick, J.P., 2017. Hf isotope evidence for variable slab input and crustal addition in basalts and andesites of the Taupo Volcanic Zone, New Zealand. Lithos. https://doi.org/10.1016/j.lithos.2017.04.009

Walker, G.P.L., Self, S., Wilson, L., 1984. Tarawera 1886, New Zealand — A basaltic plinian fissure eruption. J. Volcanol. Geotherm. Res. 21, 61–78. https://doi.org/10.1016/0377-0273(84)90016-7

Wallace, P.J., 2005. Volatiles in subduction zone magmas: concentrations and fluxes based on melt inclusion and volcanic gas data. J. Volcanol. Geotherm. Res. 140, 217–240. https://doi.org/10.1016/j.jvolgeores.2004.07.023

Wallace, P.J., Kamenetsky, V.S., Cervantes, P., 2015. Melt inclusion CO2 contents, pressures of olivine crystallization, and the problem of shrinkage bubbles. Am. Mineral. 100, 787–794. https://doi.org/10.2138/am-2015-5029

Waters, L.E., Lange, R.A., 2015. An updated calibration of the plagioclase-liquid hygrometer-thermometer applicable to basalts through rhyolites. Am. Mineral. 100, 2172–2184. https://doi.org/10.2138/AM-2015-5232

Wilson, C.J.N., Blake, S., Charlier, B.L.A., Sutton, A.N., 2006. The 26·5 ka Oruanui Eruption, Taupo Volcano, New Zealand: Development, Characteristics and Evacuation of a Large Rhyolitic Magma Body. J. Petrol. 47, 35–69. https://doi.org/10.1093/petrology/egi066

Wilson, C.J.N., Gravley, D.M., Leonard, G.S., Rowland, J. V., 2009. Volcanism in the central Taupo Volcanic Zone, New Zealand: tempo, styles and controls. Spec. Publ. IAVCEI 225–247. https://doi.org/10.1144/IAVCEL002.12

Wilson, C.J.N., Houghton, B.F., McWilliams, M.O., Lanphere, M.A., Weaver, S.D., Briggs, R.M., 1995. Volcanic and structural evolution of Taupo Volcanic Zone, New Zealand: a review. J. Volcanol. Geotherm. Res. 68, 1–28. https://doi.org/10.1016/0377-0273(95)00006-G

Wysoczanski, R.J., Wright, I.C., Gamble, J.A., Hauri, E.H., Luhr, J.F., Eggins, S.M., Handler, M.R., 2006. Volatile contents of Kermadec Arc–Havre Trough pillow glasses: Fingerprinting slab-derived aqueous fluids in the mantle sources of arc and back-arc lavas. J. Volcanol. Geotherm. Res. 152, 51–73. https://doi.org/10.1016/J.JVOLGEORES.2005.04.021

Zellmer, G.F., Kimura, J.-I., Stirling, C.H., Lube, G., Shane, P.A., Iizuka, Y., 2020. Genesis of recent mafic magmatism in the Taupo Volcanic Zone, New Zealand: insights into the birth and death of very large volume rhyolitic systems? J. Petrol. 61, egaa027. https://doi.org/10.1093/petrology/egaa027